



HAL
open science

Entanglement Spectroscopy and its application to the fractional quantum Hall phases

Nicolas Regnault

► **To cite this version:**

Nicolas Regnault. Entanglement Spectroscopy and its application to the fractional quantum Hall phases. Strongly Correlated Electrons [cond-mat.str-el]. Ecole Normale Supérieure de Paris - ENS Paris, 2013. tel-00967692

HAL Id: tel-00967692

<https://theses.hal.science/tel-00967692>

Submitted on 1 Apr 2014

HAL is a multi-disciplinary open access archive for the deposit and dissemination of scientific research documents, whether they are published or not. The documents may come from teaching and research institutions in France or abroad, or from public or private research centers.

L'archive ouverte pluridisciplinaire **HAL**, est destinée au dépôt et à la diffusion de documents scientifiques de niveau recherche, publiés ou non, émanant des établissements d'enseignement et de recherche français ou étrangers, des laboratoires publics ou privés.



**Mémoire d'Habilitation à diriger des recherches de
l'École Normale Supérieure**

présenté par

Nicolas REGNAULT

Sujet du mémoire

**Entanglement Spectroscopy and its application
to the fractional quantum Hall phases**

Soutenue le 27 mai 2013 devant le jury composé de :

Nigel Cooper (Rapporteur)
Jean Dalibard (Examineur)
Benoît Douçot (Rapporteur)
Philippe Lecheminant (Examineur)
Vincent Pasquier (Président)
Didier Poilblanc (Rapporteur)

Abstract

The entanglement spectroscopy, initially introduced by Li and Haldane in the context of the fractional quantum Hall effects, has stimulated an extensive range of studies. The entanglement spectrum is the spectrum of the reduced density matrix, when we partition the system into two. For many quantum systems, it unveils a unique feature: Computed from the bulk ground state wave function, the entanglement spectrum give access to the physics of edge excitations.

In this manuscript, we give an overview of the entanglement spectroscopy. We introduce the basic concepts through the case of the quantum spin chains. We present an extensive review of the entanglement spectra applied to the fractional quantum Hall phases, showing how much information is encoded within the ground state and how different partitions probe different type of excitations. As a practical application of this technique, we discuss how it can discriminate between the different phases that emerge in the strongly interacting Chern insulators.

Contents

1	Introduction	3
2	Entanglement spectrum	5
2.1	Definitions	5
2.2	A simple example: Two spin- $\frac{1}{2}$	7
2.3	The AKLT spin chain	8
2.4	Matrix Product States and entanglement spectrum	11
3	Fractional quantum Hall effect and entanglement spectra	13
3.1	Fractional quantum Hall effect: Overview and notations	14
3.2	Orbital entanglement spectrum	17
3.3	OES beyond model wave functions	24
3.4	Particle entanglement spectrum	27
3.5	Real space entanglement spectrum	31
4	Entanglement spectrum as a tool: Probing the Fractional Chern Insulators	33
4.1	From Chern Insulators to Fractional Chern Insulators	34
4.2	ES for FCI	37
5	Conclusion	39

1 Introduction

In the past decade it has become clear that Landau's theory of phase transitions which involves the appearance of a broken-symmetry order parameter does not apply to a series of phases of matter with so-called topological order. Topological phases exhibit the surprising property that their quantum ground state is degenerated and that no local measurement can distinguish them. This feature is the key of topological quantum computing: Using this robustness to solve the problem of local decoherence (for example due to disorder) by construction instead of quantum error correction (hardware vs software approach). This inherent robustness is also the source of a major issue: The absence of a local order parameter makes the identification of a topological order a difficult task.

The prototype of two-dimensional topologically ordered phases are the experimentally accessible fractional quantum Hall (FQH) phases. The fractional quantum Hall effect (FQHE) [1] occurs in a two dimensional electron gas at very low temperatures and strong magnetic fields. The Hall conductance as a function of magnetic field shows plateaus at values integer or fractional value ν of the quantum of conductance e^2/h . The electron liquids obtained for non-integer ν come from the strong interaction between electrons. In fact, the FQHE is one of the most famous and most difficult strongly interacting quantum system. One key feature is the possibility for these liquids of hosting quasiparticles with fractional charges and obeying fractional statistics (between fermions and bosons) or more exotic non-abelian statistics.

A promising tool to extract topological information from the ground state wave function is the entanglement entropy [2–4]. In the simplest case, we consider the bipartite entanglement between two parts A and B of the system in its ground state $|\Psi\rangle$. This partition is characterized by the reduced density matrix $\rho_A = \text{Tr}_B |\Psi\rangle\langle\Psi|$ of subsystem A , obtained by tracing out all the B degrees of freedom. Among the various entropies that have been considered as an entanglement measurement, the entanglement entropy is the most popular one (see Ref. [5] for an extensive review). It is defined as the Von Neumann entropy associated with ρ_A i.e. $\mathcal{S}_A = -\text{Tr}_A [\rho_A \ln \rho_A]$. For a system in d dimensions with a finite correlation length l , the entanglement entropy satisfies the area

law [6]

$$\mathcal{S}_A \simeq \alpha \mathcal{L}^{d-1} \tag{1}$$

$\mathcal{L} \gg l$ is the typical length that defines the size of the region A and α is a non-universal constant. The area law indicates that the dominant part of the entanglement entropy is controlled by the area (\mathcal{L}^{d-1}) that separates the two domains. Physically, it means that the entanglement between A and B is located at the interface of the two regions.

For two dimensional topological phases, Refs. [2] and [3] showed that the first correction to the area law is a topological term: $\mathcal{S}_A \sim \alpha \mathcal{L} - \gamma$. The sub-leading term γ is called the topological entanglement entropy: It is a constant for a given topologically ordered phase, $\gamma = \ln \mathcal{D}$. Here \mathcal{D} is the total quantum dimension characterizing the topological field theory describing the phase and thus the nature of the system excitations. The topological entanglement entropy appears as a way to characterize the topological order of a phase. However, its practical calculation depends on scaling arguments, which might be hard to obtain to sufficient accuracy from numerical calculations [7,8]. Moreover, it does not uniquely determine the topological order in the state.

The concept of entanglement spectroscopy have been shown to be a powerful tool to probe the topological order. The entanglement spectra (ES) have been initially introduced by Li and Haldane [9] in the context of the FQHE, stimulating an extensive range of studies. [10–24] They have also been studied and applied to a large scale of topological and non-topological phases including spin systems, [25–35] as well as topological insulators, [36–38] Bose-Hubbard models [39] or complex paired superfluids. [40] The topological entanglement entropy reduces the information contained in the reduced density matrix to a single number. The ES aims to have a deeper look at ρ_A by analyzing its full spectrum. Moreover, the partition of the system has to be thought in a broad sense: It can be done in the real space, in the momentum or Fourier space, or in the particle space. For many model states such as the Laughlin wave function [41] or the AKLT spin chain [42,43], the counting (number of non-zero eigenvalues) is exponentially lower than expected. This counting is related to the nature of the system excitations. The salient feature is that this information about the excitations is obtained only from the ground state. The ES is a way to extract this information and each type of cut reveals different aspects of these excitations.

This manuscript will try to give an overview of the entanglement spectroscopy, devoting a large part to its application to the FQHE and to similar phases. The extensive studies of the ES for these phases and the detailed understanding of ES that have been gained through these studies motivate this bias. This paper is organized as follow. Sec. 2 provides an introduction to the notations and concepts of the entanglement spectra (ES). We exemplify these notions on simple spin systems and relate ES to the matrix product state (MPS) representation. In Sec. 3, we present an extensive overview of the ES for the fractional quantum Hall effect (FQHE). We show the different bipartite partitions that were considered for these systems and the kind of information that were revealed performing the ES. Finally in Sec. 4, we discuss how the ES was used as tool to probe the phases that emerge in fractional Chern insulators (FCI).

2 Entanglement spectrum

As a first step, we discuss the concept of entanglement spectroscopy in some simple cases. We introduce the Li-Haldane conjecture in the case of the AKLT spin chain. We discuss the important situation where the number of reduced density matrix non-zero eigenvalues is massively reduced. In particular, we show the relation between the latter property and the matrix product state representation.

2.1 Definitions

Let consider a generic n -body quantum state $|\Psi\rangle$ that can be decomposed on the orthonormal basis $\{|\lambda\rangle\}$. We now assume that this basis can be written as the tensor product of two orthonormal basis $\{|\mu_A\rangle\}$ and $\{|\mu_B\rangle\}$ i.e. $\{|\lambda\rangle = |\mu_A\rangle \otimes |\mu_B\rangle\}$, providing a natural bipartition of the system into A and B . The decomposition of the state $|\Psi\rangle$ reads

$$|\Psi\rangle = \sum_{\mu_A, \mu_B} c_{\mu_A, \mu_B} |\mu_A\rangle \otimes |\mu_B\rangle \quad (2)$$

The entanglement matrix M is defined such that its matrix elements are given by $M_{\mu_A, \mu_B} = c_{\mu_A, \mu_B}$. The size of M is given by the dimension of the subspaces A and B that we denote respectively \dim_A and \dim_B . Note that we do not assume that $\dim_A = \dim_B$, and thus M

is generically a rectangular matrix. One can perform a singular value decomposition (SVD) of M . The SVD allows to write a rectangular matrix

$$M = UDV^\dagger \quad (3)$$

where U is a $\dim_A \times \min(\dim_A, \dim_B)$ matrix which satisfies $U^\dagger U = 1$ (i.e. has orthonormalized columns), V is a $\dim_B \times \min(\dim_A, \dim_B)$ matrix which satisfies $VV^\dagger = 1$ (i.e. has orthonormalized rows). D is a diagonal square of dimension $\min(\dim_A, \dim_B)$ where all entries are non-negative and can be expressed as $\{e^{-\xi_i/2}\}$.

Using the SVD, one can derive the Schmidt decomposition of $|\Psi\rangle$

$$|\Psi\rangle = \sum_i e^{-\xi_i/2} |A : i\rangle \otimes |B : i\rangle \quad (4)$$

where $|A : i\rangle = \sum_{\mu_A} U_{i,\mu_A}^\dagger |\mu_A\rangle$ and $|B : i\rangle = \sum_{\mu_B} V_{i,\mu_B}^\dagger |\mu_B\rangle$. To be a Schmidt decomposition, the states $|A : i\rangle$ and $|B : i\rangle$ have to obey $\langle A : i | A : j \rangle = \langle B : i | B : j \rangle = \delta_{i,j}$. This property is trivially verified using the identities on U and V . The Schmidt decomposition provides a nice and numerically efficient way to compute the spectrum of the reduced density matrix. Consider the density matrix of the pure state $\rho = |\Psi\rangle \langle \Psi|$, we compute the reduced density matrix of A by tracing out the degree of freedom related to B , i.e. $\rho_A = \text{Tr}_B \rho$. Using Eq. 4, we deduce that $\rho_A = \sum_i e^{-\xi_i} |A : i\rangle \langle A : i|$. Thus the spectrum of ρ_A can be obtained from the coefficient of the Schmidt decomposition or the SVD of the entanglement matrix and is given by the set $\{e^{-\xi_i}\}$. From a numerical perspective, getting the spectrum of ρ_A is more accurate using the SVD of M than a brute force calculation of ρ_A in the $\{|\mu_A\rangle\}$ basis followed by its diagonalization. In a similar way, we can obtain the reduced density matrix of B , $\rho_B = \text{Tr}_A \rho = \sum_i e^{-\xi_i} |B : i\rangle \langle B : i|$. Note that ρ_A and ρ_B have the same spectrum. While these two square matrices might have different dimensions (respectively \dim_A and \dim_B), they both have the same number of non-zero eigenvalues. This number has to be lower than or equal to $\min(\dim_A, \dim_B)$. Thus studying the properties of ρ_A for various partitions (i.e. choices of A and B) can be restricted to the cases where $\dim_A \leq \dim_B$.

With these tools and properties, we can now define the entanglement spectrum. The latter corresponds to the set $\{\xi_i\}$, the logarithm

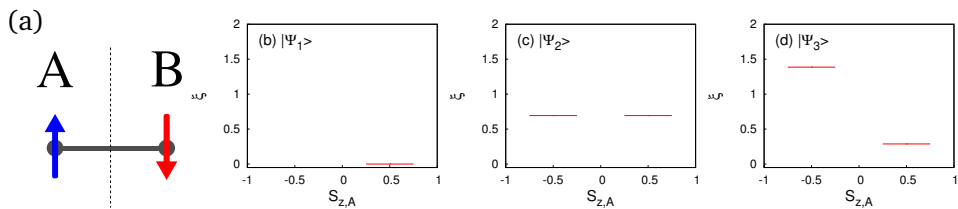


Figure 1: *From left to right:* (a) schematic picture of the two spin- $\frac{1}{2}$ system. (b) Entanglement spectrum for the state $|\Psi_1\rangle = |\uparrow\uparrow\rangle$. (c) Entanglement spectrum for the state $|\Psi_2\rangle = \frac{1}{\sqrt{2}}(|\uparrow\downarrow\rangle - |\downarrow\uparrow\rangle)$. (d) Entanglement spectrum for the state $|\Psi_3\rangle = \frac{1}{2}|\uparrow\downarrow\rangle + \frac{\sqrt{3}}{2}|\downarrow\uparrow\rangle$.

of the reduced density matrix eigenvalues. The key idea of the original article of Li and Haldane [9] was not only to look at this spectrum, but on a specific subset of these values (or a block of ρ_A) with well defined quantum numbers. Assume an operator \mathcal{O} that can be decomposed as $\mathcal{O}_A + \mathcal{O}_B$ where \mathcal{O}_A (resp. \mathcal{O}_B) only acts on the A (resp. B) subspace. One can think about \mathcal{O} as the projection of the spin operator or the momentum. If $[\mathcal{O}, \rho] = 0$, we also have $0 = \text{Tr}_B[\mathcal{O}_A, \rho] + \text{Tr}_B[\mathcal{O}_B, \rho] = [\mathcal{O}_A, \text{Tr}_B \rho] = [\mathcal{O}_A, \rho_A]$ as the trace over the B degrees of freedom of a commutator operator in the B part vanishes. If $|\Psi\rangle$ is an eigenstate of \mathcal{O} , then the latter commutes with ρ . We can simultaneously diagonalize ρ_A and \mathcal{O}_A , and label the $\{\xi_i\}$ according to the quantum number of \mathcal{O}_A .

2.2 A simple example: Two spin- $\frac{1}{2}$

To exemplify the previous notations and concepts, we consider a system of two spin- $\frac{1}{2}$ as depicted in Fig. 1a. Any state $|\Psi\rangle$ can be decomposed onto the four basis states:

$$|\Psi\rangle = c_{\uparrow\uparrow}|\uparrow\uparrow\rangle + c_{\uparrow\downarrow}|\uparrow\downarrow\rangle + c_{\downarrow\uparrow}|\downarrow\uparrow\rangle + c_{\downarrow\downarrow}|\downarrow\downarrow\rangle \quad (5)$$

A natural way to cut this system into two parts consists of the A (resp. B) part being the left (resp. right) spin. The entanglement

matrix is given by

$$M = \begin{array}{cc} & \begin{array}{l} |B : \uparrow\rangle \\ |B : \downarrow\rangle \end{array} \\ \begin{array}{l} \left(\begin{array}{cc} c_{\uparrow\uparrow} & c_{\uparrow\downarrow} \\ c_{\downarrow\uparrow} & c_{\downarrow\downarrow} \end{array} \right) & \begin{array}{l} |A : \uparrow\rangle \\ |A : \downarrow\rangle \end{array} \end{array} \quad (6)$$

where we have explicitly written which states were associated with each row and column of M . We consider three examples: A product state $|\Psi_1\rangle = |\uparrow\uparrow\rangle$, a maximally entangled state $|\Psi_2\rangle = \frac{1}{\sqrt{2}}(|\uparrow\downarrow\rangle - |\downarrow\uparrow\rangle)$ and a generic entangled state $|\Psi_3\rangle = \frac{1}{2}|\uparrow\downarrow\rangle + \frac{\sqrt{3}}{2}|\downarrow\uparrow\rangle$. The entanglement entropy for these states are respectively $\mathcal{S}_A = 0$, $\mathcal{S}_A = \ln 2$ and $\mathcal{S}_A = 2 \ln 2 - \frac{3}{4} \ln 3$.

The projection of the total spin along the z axis S_z is the sum of individual components $S_{z,A}$ and $S_{z,B}$. Thus, when performing the cut into the two parts A and B , $S_{z,A}$ is a good quantum number that can be used to label the eigenvalues of the entanglement spectrum according to the discussion in Sec. 2.1. The entanglement spectra for the three states $|\Psi_1\rangle$, $|\Psi_2\rangle$ and $|\Psi_3\rangle$ are shown in Figs. 1b-d. For the product state $|\Psi_1\rangle$, there is a single level appearing since the reduced density matrix has a single non-zero eigenvalue. For the two other examples, there are two levels, each with a given $S_{z,A}$ value. The calculation of the entanglement entropy, which is a measure of the entanglement, directly tells that $|\Psi_1\rangle$ is a product state, we can derive the same conclusion from the number of levels in the entanglement spectrum. While this example is rather a trivial result obtained from the entanglement spectrum, it stresses one of strong points of this technique. Some properties of the states can be deduced just by counting the non-zero eigenvalues of reduced density matrix.

2.3 The AKLT spin chain

We now move to a typical example of strongly correlated n -body quantum systems: The quantum spin chains. More precisely, we focus on the Affleck-Kennedy-Lieb-Tasaki (AKLT) model [42, 43]. This system is the prototype of a gapped spin-1 chain [44]. The AKLT Hamiltonian of the one dimensional spin-1 chain reads:

$$H_{\text{AKLT}} = \sum_j \vec{S}_j \cdot \vec{S}_{j+1} + \frac{1}{3} \sum_j \left(\vec{S}_j \cdot \vec{S}_{j+1} \right)^2 \quad (7)$$

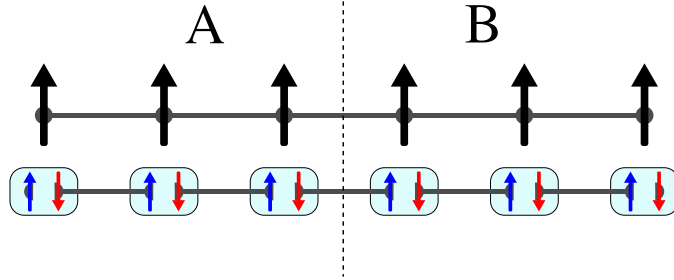


Figure 2: A schematic description of the AKLT ground state. The upper chain shows the spin-1 AKLT chain while the lower chain exhibits its valence bond description. Each spin-1 is decomposed into two spin- $\frac{1}{2}$, one red and one blue, that are projected on the triplet state (depicted by a box). The AKLT ground state is obtained by projecting one red spin- $\frac{1}{2}$ of one site with one blue spin- $\frac{1}{2}$ of the neighboring site in the singlet state. We observed the two unpaired spin- $\frac{1}{2}$, one at each end of the spin chain. This figure also shows how the system is cut into two parts A and B when performing the entanglement spectrum calculation.

The ground state of the AKLT Hamiltonian is a valence bond state. It can be understood within a simple picture sketched in Fig. 2. Each spin-1 can be written as two spin- $\frac{1}{2}$ combined in the triplet state. Between two neighboring sites, two of the four spin- $\frac{1}{2}$ (one per site) are combined in the singlet sector. When an open chain is considered, the two extreme unpaired spin- $\frac{1}{2}$ (see Fig. 2) correspond to the edge excitations, leading to a four-fold degenerate ground state (one singlet state and one triplet state).

To compute the entanglement spectrum of the AKLT ground state for an open chain, we first have to decide which of the four degenerate state we would like to analyze. In the sector of total spin $S_z = \pm 1$, there is only one state so the choice is simple, while in the sector $S_z = 0$, there are two states. For sake of simplicity we focus on the $S_z = 1$ case. To cut the system into two parts, we can follow the same procedure than the one described in the Sec. 2.2: The A part will be made of the l_A consecutive leftmost sites and the B part by the remaining rightmost sites (see Fig. 2).

Fig. 3a displays the entanglement spectrum for a AKLT open chain

2 ENTANGLEMENT SPECTRUM

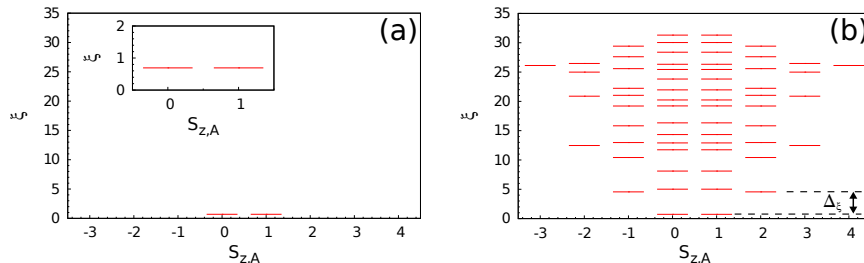


Figure 3: *Left panel:* The entanglement spectrum for the AKLT ground state with 8 sites in the $S_z = 1$ sector. The system is cut into two equal parts of size $l_A = 4$. The entanglement spectrum only contains two levels, i.e. two non zero eigenvalues in the reduced density matrix. This reflects the edge excitation (a spin- $\frac{1}{2}$) of the AKLT ground state. The inset is a zoom on these two levels. *Right panel:* The entanglement spectrum for the Heisenberg spin-1 chain with 8 sites in the $S_z = 1$ sector. The system is cut in a similar way to the AKLT case. The two lowest entanglement energy states (i.e. the two largest eigenvalue of the reduced density matrix) are similar to those of the AKLT ground state. We show the entanglement gap Δ_ξ between the similar to the part of entanglement spectrum AKLT ground state and the higher the entanglement energy states.

with 8 sites and $l_A = 4$. The entanglement energies ξ are plotted versus $S_{z,A}$, the z -projection of the A part total spin. The reduced density matrix has only two non-zero eigenvalues whereas the size of reduced density matrix is 81×81 . This dramatic reduction of the number of non-zero eigenvalues compared to a random state, is a major characteristic that we will observe for many model states. If one thinks about the cut as an artificial edge we have introduced in the system, the physical interpretation becomes obvious: What we observe here is a spin- $\frac{1}{2}$ edge excitation of the AKLT chain. This is the first example where the Li-Haldane conjecture [9] can be observed: For this gapped phase, the entanglement spectrum is directly related to the spectrum of the edge excitation. Note that the true edge excitations of the system do not play any role here since our choice of the AKLT ground state in the $S_z = 1$ sector freezes these excitations.

The AKLT Hamiltonian being the prototype of the gapped quantum spin-1 chain, it is interesting to look at the behavior entanglement

spectrum away from this specific case. The simplest case one can consider is the Heisenberg spin-1 chain where the Hamiltonian is just given by $H = \sum_j \vec{S}_j \cdot \vec{S}_{j+1}$. In Fig. 3b, we consider a similar situation than the one for the AKLT model of Fig. 3a. At the bottom of the entanglement spectrum, we recover two states, with the same quantum numbers than the AKLT case. Contrary to the latter, we also observe some higher entanglement energy levels. The AKLT ground state and the Heisenberg spin-1 chain being adiabatically connected, we would like to argue that the low entanglement energy structure in the Heisenberg spin-1 entanglement spectrum will characterize the system. We define the entanglement gap Δ_ξ as the minimum difference of entanglement energy level between the low entanglement energy structure similar to a model state (the AKLT model in this example) and the entanglement energy levels above this structure. The meaning of Δ_ξ is actually the Li-Haldane conjecture away from model states: If this entanglement gap stays finite in the thermodynamical limit, the edge excitations of the system will be in the same universality class than the model state whose entanglement spectrum reduces to the same low entanglement energy structure.

To summarize, this example has already been able to show us several features of the entanglement spectrum. For some model states, the number of non-zero eigenvalues might be related to the edge excitation of the system. This number can be exponentially smaller than one can expect from a random state, which is a non-trivial signature. Away from this ideal situation and as long as one stays in the same universality class, we would expect to observe a similar fingerprint than the model state in the low entanglement energy part of the spectrum. This structure should be protected from the higher entanglement energy levels by an entanglement gap.

2.4 Matrix Product States and entanglement spectrum

The understanding and simulation of quantum many-body states in one space dimension has experienced revolutionary progress with the advent of the density matrix renormalization group [45]. In modern language, this method can be viewed as a variational optimization over the set of matrix product states (MPS) [46, 47]. Let consider a quantum state $|\Psi\rangle = \sum_{\{m_i\}} c_{\{m_i\}} |m_1, \dots, m_{N_{\text{orb}}}\rangle$, where the $\{m_i\} = \{m_1, \dots, m_{N_{\text{orb}}}\}$ are a set of physical indices such as a spin

up or down, an occupied or empty orbital, ...

$$|\Psi\rangle = \sum_{\{m_i\}} (C^{[m_1]} \dots C^{[m_{N_{\text{orb}}}]})_{\alpha_L, \alpha_R} |m_1, \dots, m_{N_{\text{orb}}}\rangle \quad (8)$$

where the $\{C^{[m]}\}$ is a set of matrices (each orbital might require a different set of matrices) and α_L and α_R are boundary conditions that pick one matrix element of the matrix product (taking the trace being another option). The $C_{\alpha, \beta}^{[m]}$ matrices have two types of indices. $[m]$ is the physical index and (α, β) are the bond indices (or auxiliary space indices) where $\alpha, \beta = 1, \dots, \chi$. χ is called the bond dimension. Such a rewriting of a state decomposition is always possible. When the bond dimension χ of the matrix $C^{[m]}$ is much smaller than the size of the n -body Hilbert space, this formulation provides a more economical representation of the state. The crucial question is how small can χ be for Eq. 8 to still be an exact statement. Generic 1-D gapped systems can be approximated by finite χ [48]. Critical systems however require an MPS with an infinite bond dimension [49, 50].

The AKLT ground state that we have discussed in the previous section can be expressed in a rather simple MPS form. In that case, N_{orb} is the number of spin-1, the physical index m can take three different values $-1, 0, +1$ corresponding to the three values of S_z . The MPS representation requires three 2×2 matrices

$$C^{[0]} = \begin{pmatrix} -\sqrt{\frac{1}{3}} & 0 \\ 0 & \sqrt{\frac{1}{3}} \end{pmatrix}, \quad C^{[+1]} = \begin{pmatrix} 0 & \sqrt{\frac{2}{3}} \\ 0 & 0 \end{pmatrix}, \quad (9)$$

$$C^{[-1]} = \begin{pmatrix} 0 & 0 \\ -\sqrt{\frac{2}{3}} & 0 \end{pmatrix}.$$

In this example, the size of the $C^{[m]}$ matrices is equal to the number of non zero eigenvalues observed in the entanglement spectrum. As we will now show, these two quantities are related. A way to create a bipartite partition of the system is to consider A being made of the indices $\{m_1, \dots, m_{l_A}\}$ and B built from the indices $\{m_{l_A+1}, \dots, m_{N_{\text{orb}}}\}$. Following the notations of Eq. 2, we have $\{|\mu_A\rangle = |m_1, \dots, m_{l_A}\rangle\}$ and $\{|\mu_B\rangle = |m_1, \dots, m_{N_{\text{orb}}}\rangle\}$. The MPS formulation of Eq. 8 can be rewritten to

make this partition apparent

$$|\Psi\rangle = \sum_{\alpha=1}^{\chi} \sum_{\{m_i\}} (C^{[m_1]} \dots C^{[m_{l_A}]})_{\alpha_L, \alpha} (C^{[m_{l_A+1}]} \dots C^{[m_{N_{\text{orb}}}]})_{\alpha, \alpha_R} |m_1, \dots, m_{N_{\text{orb}}}\rangle \quad (10)$$

Thus we obtain that

$$|\Psi\rangle = \sum_{\alpha=1}^{\chi} |A : \alpha\rangle \otimes |B : \alpha\rangle \quad (11)$$

with

$$|A : \alpha\rangle = \sum_{\{m_i\}} (C^{[m_1]} \dots C^{[m_{l_A}]})_{\alpha_L, \alpha} |m_1, \dots, m_{l_A}\rangle \quad (12)$$

$$|B : \alpha\rangle = \sum_{\{m_i\}} (C^{[m_{l_A+1}]} \dots C^{[m_{N_{\text{orb}}}]})_{\alpha, \alpha_R} |m_{l_A+1}, \dots, m_{N_{\text{orb}}}\rangle \quad (13)$$

While this decomposition looks similar to the Schmidt decomposition in Eq. 4, the states $|A : \alpha\rangle$ and $|B : \alpha\rangle$ are neither orthonormal nor linearly independent. Some extra steps are actually required to obtain the true Schmidt decomposition. Still, the key relation between the entanglement spectrum and the MPS is already visible at this stage: No matter what are these necessary extra steps, the bond dimension χ cannot be lower than the number of non-zero eigenvalues of the reduced density matrix. The latter number gives the optimal size for the MPS representation of a state (as discussed in the case of the AKLT ground state). Thus any massive reduction of the system entanglement spectrum should be the sign of an efficient MPS representation.

3 Fractional quantum Hall effect and entanglement spectra

In this section, we review the different aspects of entanglement spectra applied to the fractional quantum Hall effect. We provide a short (and partial) introduction to this topic. We discuss the different partitions that have been proposed and their relation. In particular, we show how much information about the excitations can be extracted from the ground state by using the entanglement spectra.

3.1 Fractional quantum Hall effect: Overview and notations

In this manuscript, we restrict to the case of spinless particles occupying the lowest Landau level. The natural geometry to consider is the plane (or disk). For technical reasons, other geometries having periodic boundary conditions such as the cylinder [51], the torus [52] or the sphere [53], are more convenient when it comes to finite size (numerical) studies. In the following, we will mostly focus on the genus zero surfaces and in particular the disk and the sphere. We note N the number of particles in the system and N_Φ the number of flux quanta. The filling factor is defined (in the thermodynamical limit) as $\nu = N/N_\Phi$. A convenient choice for the one-body basis on the plane (using the symmetric gauge) and on the sphere leads to the following set of wave functions:

$$\phi_m(\mathbf{r}) = \begin{cases} \frac{1}{\sqrt{2\pi 2^m m!}} z^m e^{-\frac{1}{4}|z|^2} & \text{plane} \\ \sqrt{\frac{(N_\Phi+1)!}{4\pi m!(N_\Phi-m)!}} u^m v^{N_\Phi-m} & \text{sphere} \end{cases} \quad (14)$$

On the plane (or disk) $z = x + iy$ is the particle coordinate, $L_z = m$ is the angular momentum (where $m \geq 0$ is an integer). On the sphere, $u = \cos(\theta/2)e^{i\varphi/2}$ and $v = \sin(\theta/2)e^{-i\varphi/2}$ are the spinor coordinates on the sphere with the polar coordinates (θ, φ) , and $L_z = N_\Phi/2 - m$ is the angular momentum along z where $m = 0, 1, \dots, N_\Phi$. N_Φ is the number of flux quanta that pierce through the sphere. On such a closed geometry, both the radius ($\propto \sqrt{N_\Phi}$) of the sphere and the number of orbitals ($N_\Phi + 1$) are fixed by the strength of the magnetic monopole at its center. Figs 4a and 4b schematically describe these orbitals for both geometries.

On the plane geometry, a general quantum Hall wave function for N particles in the lowest Landau level can be expressed as

$$\Psi(z_1, \dots, z_N) = P(z_1, \dots, z_N) e^{-\frac{1}{4}\sum_i |z_i|^2} \quad (15)$$

where P is a polynomial in the N complex variables associated with the particle positions z_1, \dots, z_N . If we restrict to fermionic wave function, this polynomial has to be anti-symmetric. Note that any wave function written on the disk can also be obtained using the stereographic projection by identifying $z \simeq u/v$ (up to some global factor). So when discussing model wave function on the plane or the sphere geometry,

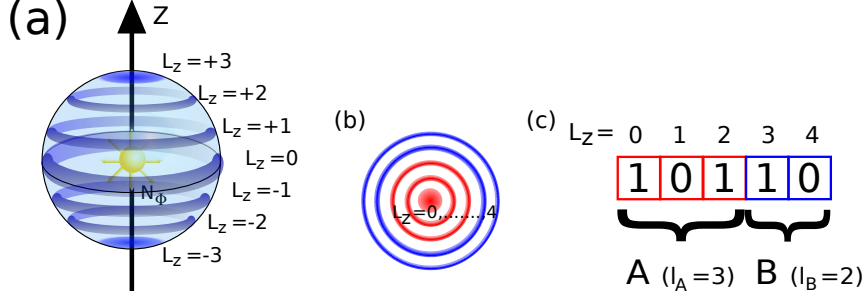


Figure 4: Schematic representation of the orbital basis (a) on the sphere geometry for $N_\Phi = 3$ and (b) on the disk geometry. (c) We show a typical n -body state of the occupation basis having three particles in orbital with angular momentum $L_z = 0, 2$ and 3 . When we perform an orbital partition into the l_A leftmost orbitals (denoted in red here), the A part in real space is roughly the domain that contains the three red orbitals.

it is sufficient to provide P and we can drop all the other factors. We can decompose this wave function in the occupation basis, using the orbitals of Eq. 14

$$\Psi(z_1, \dots, z_N) = \sum_{\{\lambda\}} c_\lambda \mathcal{M}_\lambda(z_1, \dots, z_N) \quad (16)$$

\mathcal{M}_λ is the normalized Slater determinant that has its orbital occupation given by the configuration λ (such a configuration is shown in Fig. 4c). The functions \mathcal{M}_λ form a set of orthonormal free many-body states. When the wave function is obtained through numerical simulation, such a decomposition is directly accessible: One diagonalizes an Hamiltonian by expressing it in a convenient basis which is generally the occupation basis for the FQHE. For model wave functions such as the Laughlin [41] or Moore-Read [54] states, One can use an efficient recursive algorithm [55] that provides the corresponding decomposition.

The archetype of FQH model wave function is the celebrated Laughlin state [41]

$$\Psi_{\text{Lgh}}(z_1, \dots, z_N) = \prod_{i < j} (z_i - z_j)^m e^{-\frac{1}{4} \sum_i |z_i|^2} \quad (17)$$

3 FRACTIONAL QUANTUM HALL EFFECT AND ENTANGLEMENT SPECTRA

m is the only variational parameter. Actually, m is related to the filling factor $\nu = 1/m$. On the sphere geometry, Eq. 17 implies the relation $N_\Phi = m(N - 1)$. For a fermionic wave function, m has to be odd. $m = 1$ corresponds to the completely filled lowest Landau level. It is a single Slater determinant (Vandermonde determinant) and thus is a product state in the occupation basis. At $\nu = 1/3$, the Laughlin wave function is a very accurate approximation of the FQH ground state obtained through any realistic simulation. Being a topological phase in its full glory (as opposed to the integer quantum Hall effect), the Laughlin wave function is degenerate when placed on a higher genus surface. For example, it is m -fold degenerate on the torus geometry.

Bulk excitations can be nucleated by removing (for quasielectron) or inserting (for quasihole) fluxes. Each excitation carries a fractional charge ($\pm e/m$) and obeys fractional statistics. For one quasihole located at the position η , we can write the corresponding wave function

$$\Psi_{\text{Lgh,1qh}}(z_1, \dots, z_N; \eta) = \prod_i (z_i - \eta) \Psi_{\text{Lgh}}(z_1, \dots, z_N) \quad (18)$$

Changing the quasihole position η spans a subspace described by a basis of $N + 1$ quasihole states, each of them having a well and unique defined angular momentum. More generally, the number of quasihole states for given values of N and N_Φ is a signature of the phase and acts as a fingerprint that can be tracked in numerical simulations. This counting of states can be obtained by the Haldane's exclusion principle (or Haldane statistics). For the $\nu = 1/m$ Laughlin, this number is identical to the number of configurations with N particles and $N_\Phi + 1$ orbitals where there is no more than 1 particle in m consecutive orbitals. Fig. 5 give some simple examples of compatible configurations. Note that both the Laughlin wave function and its quasihole excitations are the only zero energy states of a local two-body model interaction [53], Eq. 18 being among them the unique densest zero energy state.

The edge excitations of the Laughlin state are described by a chiral $U(1)$ boson. For an edge of length \mathcal{L} , the dispersion relation is given by $E \simeq \frac{2\pi v}{\mathcal{L}} n$ where n is an integer, v is the edge mode velocity. The degeneracy of each energy level can be deduced from the picture described in Fig. 6. Using the Haldane statistics for the Laughlin $\nu = 1/m$ state, starting from the ground state, we obtain the sequence 1, 1, 2, 3, ... irrespective of m . Like in the case of the quasihole state, this counting is a fingerprint of the edge excitations.

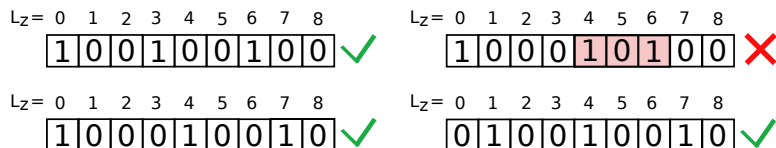


Figure 5: An example of the Haldane's exclusion principle. We consider a system with $N = 3$ particles in 9 orbitals on the disk with momenta going from $L_z = 0$ to $L_z = 8$. Among the four configurations described here, only three of them satisfy the Haldane's exclusion principle of the $\nu = 1/3$ Laughlin: No more than one particle in three consecutive orbitals. The violation of this principle in the top right configuration is shown in light red. For each compatible partition, one can easily compute the corresponding total L_z value (for example 9 for the left topmost configuration).

Finally, we give another example of model wave functions: The Moore-Read state [54]. This model is considered to be the prototype model wave function to explain the appearance of a Hall conductance plateau at filling factor $\nu = 5/2$ (i.e. in the second Landau level). It can be written as

$$\Psi_{\text{MR}}(z_1, \dots, z_N) = \text{Pf} \left(\frac{1}{z_i - z_j} \right) \prod_{i < j} (z_i - z_j)^2 e^{-\frac{1}{4} \sum_i |z_i|^2} \quad (19)$$

The Moore-Read state possesses two kind of excitations: Abelian excitations with a charge $\pm e/2$ and non-Abelian excitations carrying a charge $\pm e/4$. In a similar way to the Laughlin case, the number of quasihole states can be derived from the Haldane's exclusion principle (in that case, no more than 2 particles in 4 consecutive orbitals). The Moore-Read state has two edge modes: a charge edge mode similar to the one of the Laughlin state and a neutral Majorana fermion edge mode. Note that a natural way to build the Moore-Read state is based on the conformal field theory (CFT) [54], rewriting Eq. 19 as a correlator (using the CFT of the Ising model in that present case).

3.2 Orbital entanglement spectrum

Li and Haldane [9] proposed to compute the ES of a FQH state using a partition in orbital basis. We call this type of ES the orbital en-

3 FRACTIONAL QUANTUM HALL EFFECT AND ENTANGLEMENT SPECTRA

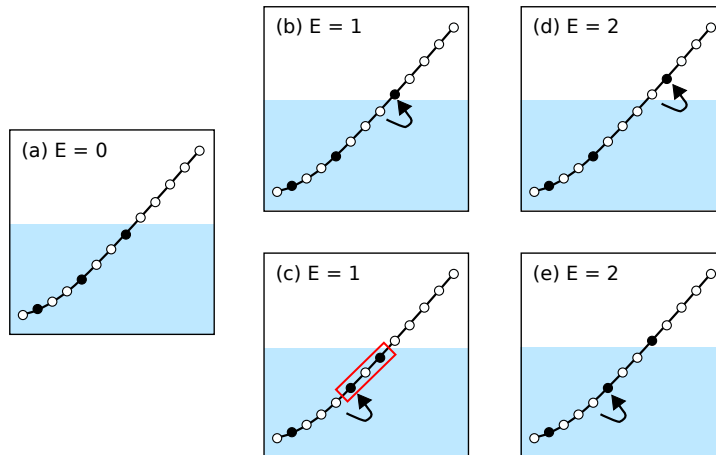


Figure 6: A description of the chiral $U(1)$ edge mode counting at $\nu = 1/3$. (a) The ground state with energy $E = 0$. It obeys the Haldane statistics (no more than one particle in three consecutive orbitals). The light blue denotes the filled Fermi sea. (b) The lowest energy excitation ($E = 1$) that satisfies the Haldane statistics. (c) An example of an excitation at the same energy but violating (in red) the Haldane statistics. (d) and (e) The two possible excitations at $E = 2$.

tanglement spectrum (OES). As already pointed out in Ref. [7] where the authors tried to extract the topological entanglement entropy of the Laughlin state from the wave function, a cut in the orbital basis roughly mimics a cut in real space. The OES is defined by the number of consecutive orbitals that are considered. This number will be denoted l_A , the number of orbitals for the B part being l_B satisfying $l_A + l_B = N_\Phi + 1$ on the sphere geometry. When we compute the OES for a FQH state on the geometry such as the sphere or the disk, one can use two good quantum numbers to label the blocks of the reduced density matrix: N_A the number of particles in A and $L_{z,A}$ the projection of the total angular momentum of the particles in A . The OES is generally represented as the entanglement energies ξ as a function of $L_{z,A}$ for a fixed value of N_A . A typical example is available in Fig. 7 for the $\nu = 1/3$ Laughlin state. Note that for sake of simplicity and as opposed to many of the original publications, the non-trivial part

of the OES is located at the left hand side of the plot. We also shift the origin of $L_{z,A}$ such that the leftmost entanglement level state has $L_{z,A} = 0$.

The OES of the Laughlin state is highly specific: Any random state with the same symmetry would produce much more entanglement energy levels, i.e. it would have much less zero eigenvalues in the reduced density matrix. Actually, not only additional entanglement energy levels would be present in sector of $L_{z,A}$ where there is no level for the Laughlin state, but the total number of level would be exponentially larger. Thus such a model state induces large constraints on the reduced density matrix. In Fig. 7, we observe that the counting of entanglement energies starting from the left matches the sequence 1, 1, 2, 3, 5, 7, 11. This is the expected counting sequence for a chiral $U(1)$ boson edge mode as discussed in Sec. 3.1. Beyond a given $L_{z,A}$, the OES counting starts being lower than the $U(1)$. Knowing we are dealing with a finite size system (both in the number of orbitals and particles), there is a maximum value of $L_{z,A}$ that can be reached and there is single state with l_A orbitals and N_A fermions that can reach it. Thus it is clear than both countings should differ at some point since the $U(1)$ counting keeps growing. We name the thermodynamical region the part of the OES where no size effect affects the edge mode counting. This region increases with the system size. In a simplified picture, we can think about the unique state at $L_{z,A} = 0$ of the OES as a Laughlin liquid droplet for N_A particles. Slightly increasing $L_{z,A}$ corresponds to generate edge mode excitations. A more robust foundation to this schematic point of view will be described in Sec. 3.4.

From this observation, Li and Haldane conjectured that in the thermodynamical limit the OES should be identical to the energy spectrum of the edge mode of the model state. This statement goes beyond the counting argument which is in itself a signature of the edge physics. To corroborate this idea, one can look at the evolution of the entanglement energies when we increase the system size [13]. These energies should mimic the dispersion relation of the gapless edge mode $\frac{2\pi v}{\mathcal{L}} L_{z,A}$ where \mathcal{L} is the cut perimeter. Despite some indication that this description is correct, the finite size calculations are unable to make a definitive conclusion. A more accurate approach will be discussed in Sec. 3.5, and will provide more convincing evidences of this conjecture.

A similar calculation can be performed on other geometries. Figs 8a-

3 FRACTIONAL QUANTUM HALL EFFECT AND ENTANGLEMENT SPECTRA

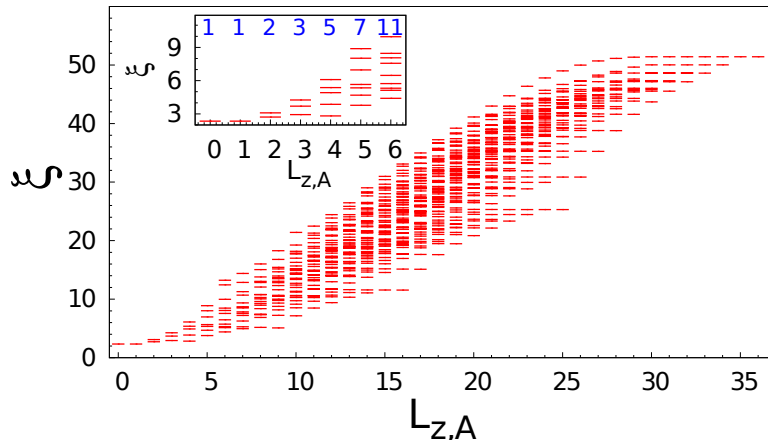


Figure 7: OES for the $\nu = 1/3$ Laughlin with $N = 12$ fermions on the sphere geometry, keeping $l_A = 17$ orbitals and looking at the fixed number of particles sector $N_A = 6$. The inset provides a zoom on the entanglement spectrum related to the $U(1)$ edge mode counting of the Laughlin state. As expected this counting is 1, 1, 2, 3, 5, 7, 11. For this cut, the deviation of the OES counting to the edge mode counting (due to finite size effects) starts at $L_{z,A} = 7$: The OES gives 13 levels while the $U(1)$ counting is 15.

d shows the OES of the $\nu = 1/3$ Laughlin state for the disk, the cylinder and the thin annulus (or conformal limit [13]). While the shape of the OES depends on the geometry, the counting remains identical as long as one considers genus zero surfaces. The OES on the two different cylinder in Figs 8c and 8d are a clear consequence of the area law. While the OES is an approximation of a real space cut, its shape depends on the length of the cut. On the cylinder, this length is controlled by the circumference (or perimeter), and does not vary with the number of flux quanta N_Φ (the usual hemisphere cut for the sphere would give a length proportional to $\sqrt{N_\Phi}$). A smaller perimeter and thus a smaller entanglement entropy, results in an OES with a steeper slope.

Moving to a higher genus surface like the torus leads to a slightly different picture [12]. The usual orbital basis on the torus is translational invariant along one direction of this geometry. Performing the bipartite partition gives rise to two artificial and spatially separated edges. The OES mimics the physics of two counter-propagating edge

3.2 Orbital entanglement spectrum

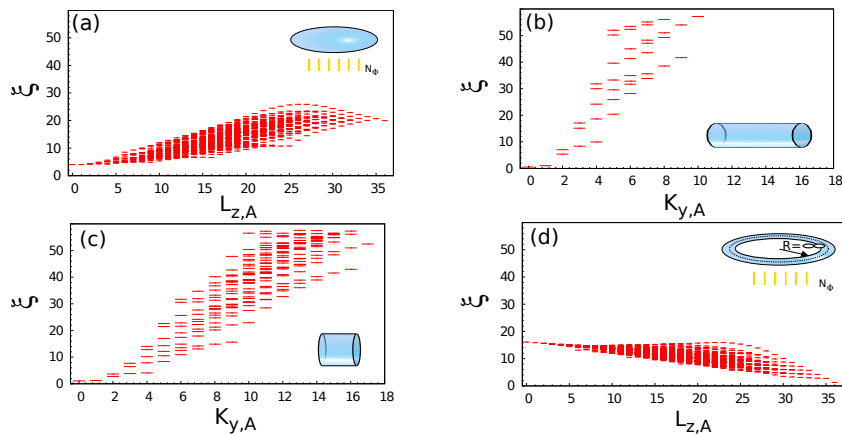


Figure 8: *From left to right, top to bottom:* Orbital entanglement spectrum for the $\nu = 1/3$ Laughlin with $N = 12$ fermions, keeping $l_A = 17$ orbitals and looking at the fixed number of particles sector $N_A = 6$, on different geometries: The disk geometry (a), a thin cylinder with a perimeter of $L = 10l_B$ (b), a thicker cylinder with a perimeter of $L = 15l_B$ (c) and the thin annulus limit (d). Note that for the cylinder geometry, we use the momentum along the cylinder perimeter $K_{y,A}$ instead of the angular momentum $L_{z,A}$.

modes. A consequence of this interplay between these two modes is the absence of zero eigenvalue in the reduced density matrix. This is a major difference with the OES for the genus zero geometries.

Beyond the thermodynamical region of the OES, finite size effects start to appear. There, the spectrum also has a non-trivial structure compared to a generic wave function. For most of the model wave function, there is no quantitative understanding of this non-thermodynamical part of the OES. In the case of the $\nu = 1/m$ Laughlin state, it was shown [15] that the counting of this region can actually be deduced from a generalized exclusion principle that depends on m . Actually, it is a nice example where finite size effects allow to get more information than the thermodynamical limit: While all $\nu = 1/m$ Laughlin states have the same edge theory, a chiral $U(1)$ boson, the compactification radius of the bosons depends on m (\sqrt{m} in that case). The thermodynamical region gives access to the $U(1)$ counting whereas the finite size effects encode the value m .

3 FRACTIONAL QUANTUM HALL EFFECT AND ENTANGLEMENT SPECTRA

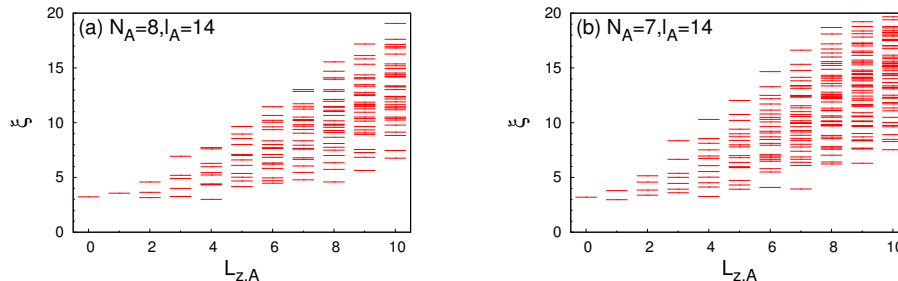


Figure 9: OES for the $\nu = 2 + 1/2$ Moore-Read state with $N = 16$ fermions keeping $l_A = 14$ orbitals. (a) Setting $N_A = 8$ we observe the counting $1, 1, 3, 5, \dots$ which is related to the vacuum sector. (b) Setting $N_A = 7$, another counting emerges $1, 2, 4, 7, \dots$ corresponding to the non-Abelian sector. In both cases and for this system size, the counting starts to deviate from the CFT one starting from $L_z = 4$.

More complex model wave functions exhibit a richer OES structure. We focus on the Moore-Read state. Figs. 9a and 9b give the OES for this state using the same partition (here $l_A = 14$) but looking at two different blocks of the reduced density matrix, namely $N_A = 8$ for Fig. 9a and $N_A = 7$ for Fig. 9b. For these two cases, the counting in the thermodynamical region is different, reflecting the two sectors of the CFT used to build this state. A surprising result here is that the state itself is built only using one of the two sectors, whereas the OES exhibits both.

For the time being, we have only looked at the OES for the ground state (i.e. in the absence of excitations) of model wave functions. But the OES in presence of pinned excitations is also quite insightful [56]. Fig. 10 shows the OES for the Moore-Read state in presence of pinned quasihole excitations. In order to preserve the rotation symmetry along the z axis of the sphere, the excitations are located at the poles. We consider two situations: One Abelian excitation of charge $e/2$ is located at the north pole in the hemisphere A (Fig. 10a) and two non-Abelian excitations, each carrying a charge $e/4$, one at each pole (Fig. 10b). In both cases, the system has the same number of particles and flux quanta, and the OES is computed for the same parameters for l_A and

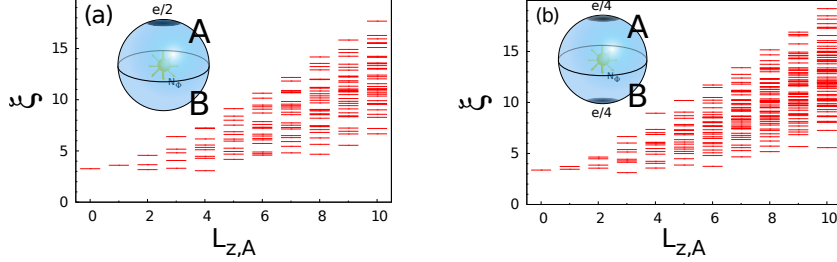


Figure 10: Orbital entanglement spectrum for the $\nu = 2 + 1/2$ Moore-Read state with quasiholes for $N = 16$ fermions and $N_\Phi = 30$ flux quanta, keeping $N_A = 8$ particles and $l_A = 15$ orbitals. We show two different situations: (a) one Abelian excitation of charge $e/2$ is located at the north pole in the hemisphere A , (b) two non-Abelian excitations, each carrying a charge $e/4$, one at each pole. Both situations clearly exhibit a different counting.

N_A . Still, the OES clearly exhibits a different counting: For Fig. 10a we recover the counting of the vacuum sector (like Fig. 9a) and for Fig. 10b we recover the counting of the non-Abelian sector (like Fig. 9b). Thus the OES can be used as a probe to check the parity of the number of non-Abelian excitations in a region of the system. Note that the OES of the Laughlin state is not modified by the presence of pinned quasihole excitations.

As a final note about the OES for model wave functions, we should stress once again that the rank of the reduced density matrix being exponentially smaller than any random state with the same symmetry is a major property. We have discussed in Sec. 2.4 that such a feature is a signal that an efficient MPS formula might exist. In the case of the FQHE, the edge modes are gapless. The ES reflecting the edge physics, we expect this MPS to be infinite, as opposed to the AKLT example. Indeed, recent developments [57, 58] have shown that an (infinite) MPS formulation was available for a large class of model wave functions, with a well controlled truncation parameter that allows numerical calculations.

3.3 OES beyond model wave functions

While the OES has already allowed to get some insight on the information encoded within the ground state of a topological phase, we would like to use it as a probe to detect topological order. For that purpose, we need to move away from model state. When dealing with more realistic description of FQH systems, several assumptions are made. In general, we suppose that there is no Landau level mixing, and in many cases we also assume that electrons are spin polarized. For low filling factor (such as $\nu = 1/3$) these hypothesis are quite accurate. Moreover, the disorder is neglected. In this scenario and for $\nu < 1$, the effective Hamiltonian reads

$$\mathcal{H} = \mathcal{P}_{\text{LLL}} \sum_{i < j} V(\vec{r}_i - \vec{r}_j) \mathcal{P}_{\text{LLL}} \quad (20)$$

\mathcal{P}_{LLL} is the projector onto the lowest Landau level. The two particle interaction V has to be thought as the effective interaction, including effects such as screening, finite confinement of the electron gas,... In a crude approach, it is generally assumed that this interaction is just the 3-dimensional Coulomb interaction, $V(\vec{r}) = \frac{1}{r}$. The ground state of this Hamiltonian can be computed for a small number of particles and flux quanta using exact diagonalization techniques such as the Lanczos algorithm.

In Fig. 11, we have computed the OES for the ground state of the projected Coulomb interaction $|\Psi_{\text{exact}}\rangle$, using exact diagonalization. The overlap between this state and the $\nu = 1/3$ Laughlin state $|\Psi_{\text{Lgh}}\rangle$ is $|\langle \Psi_{\text{exact}} | \Psi_{\text{Lgh}} \rangle|^2 = 0.9819$. In the low entanglement energy part of the spectrum, we clearly distinguish a structure similar to the one of the Laughlin state in Fig. 7 that we have related to the edge mode excitations. As opposed to the example of the spin-1 Heisenberg model discussed in Sec. 2.3, the entanglement gap does not extend along all momentum sectors. But the edge mode counting is clearly separated from the higher entanglement energy levels. The low energy part related to the edge physics of the mode state is called the universal part of the ES. The higher energy part is dubbed the non-universal part of the ES. In this example, the idea of looking at the entanglement spectrum per momentum sector is crucial: Without resolving the OES as a function of $L_{z,A}$, the entanglement gap would not be visible.

The fact that the entanglement gap Δ_ξ does not spread over the

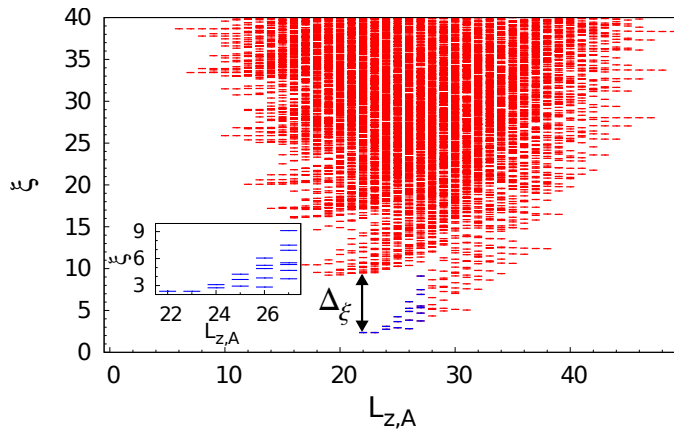


Figure 11: OES for the ground state of the Coulomb interaction with $N = 12$ fermions and $N_\Phi = 33$ on the sphere geometry, keeping $l_A = 17$ orbitals and looking at the fixed number of particles sector $N_A = 6$. We use the same system size and parameters than the OES of the $\nu = 1/3$ Laughlin in Fig. 7. The levels in blue are those that are related to the edge mode of the Laughlin state. Δ_ξ denotes the entanglement gap between the edge mode counting and the non-universal part of the spectrum. The inset provides a zoom on the entanglement spectrum related to the $U(1)$ edge mode counting of the Laughlin state.

full spectrum could appear as a failure of the OES to find the universality class. First we should focus on the part of the spectrum that has reached the thermodynamical limit, i.e. in the Li and Haldane picture the region that should match the edge physics. From that perspective, what should be relevant is the presence of the entanglement gap in this region that grows when we increase the system size. In the article that has introduced the ES [9], convincing numerical results were provided that Δ_ξ does not collapse when the system size is increased. Moreover, the extension of region where there is an entanglement gap tightly depends on the geometry in finite size calculations. For example, performing the OES of the same state but on a thin annulus (also called the conformal limit [13]) leads to a modified picture as shown in Fig. 12. In some cases, one clearly separates the full universal part (the one of some model state) from the non-universal of the ES. As

3 FRACTIONAL QUANTUM HALL EFFECT AND ENTANGLEMENT SPECTRA

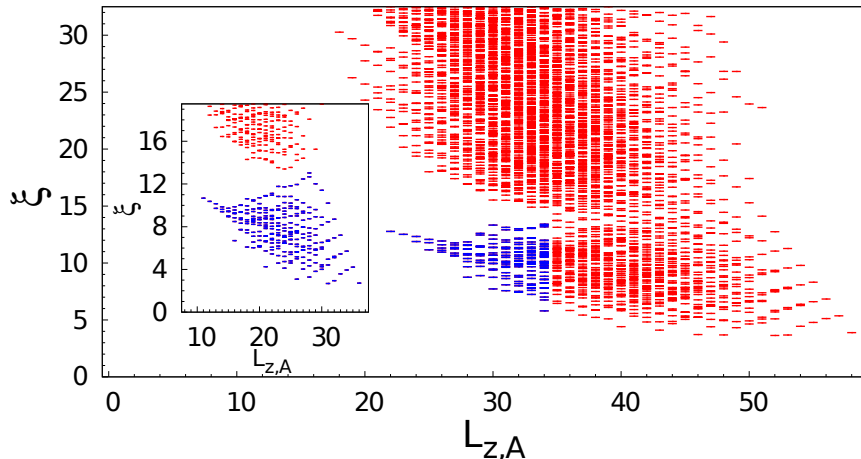


Figure 12: OES for the ground state of the Coulomb interaction on the thin annulus geometry, with the same system size and parameters than in Fig. 11. The levels in blue have an identical counting than the one of the Laughlin state and is separated from the non-universal part of the spectrum. The inset shows the OES for the same kind of system but with a lower number of particles ($N = 10$). In that case, the structure associated with the Laughlin state (in blue) clearly detaches from the non-universal part.

discussed in Ref. [13], this can happen even when the exact state has a moderate overlap with the model state. In some examples, one can even adiabatically go from the model state to the exact state without closing the entanglement gap.

Until now, we have mostly focused on the universal part of the ES. Looking at the Fig. 13, we observe that the non-universal part exhibits several branches. Indeed, these branches can be related to the neutral excitations (the excitations that do not involve to change the number of particles or the number of flux quanta) of the system [18]. For the FQHE, these neutral excitations are quasihole-quasielectron excitons. Two approaches are available to test this idea. One can build an approximation of the exact ground state based on the model state and the lowest energy neutral excitation that has the same symmetry than both the model and the exact states (see Fig. 14a). The other

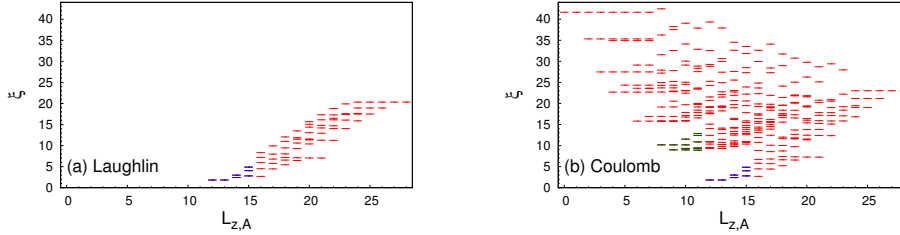


Figure 13: OES for $N = 8$ fermions and $N_\Phi = 21$ flux quanta on the sphere geometry, setting $N_A = 4$ and $l_A = 11$. (a) OES of the $\nu = 1/3$ Laughlin state. (b) OES of the ground state of the Coulomb ground state. We clearly observe three branches, the lowest (in blue) being related to the $\nu = 1/3$ Laughlin state. The second lowest branch is denoted in green.

option is to consider the model state but in finite temperature where the full density matrix is given by

$$\rho = \frac{1}{\sum_n e^{-\beta E_n}} \sum_n e^{-\beta E_n} |\Psi_n\rangle \langle \Psi_n| \quad (21)$$

where the $|\Psi_n\rangle$ and E_n are respectively the eigenstates and the eigenvalues of the Hamiltonian that produces the model state (see Fig. 14b). In both cases, we see that the resulting OES correctly captures the non-universal part. This exercise also appears to support the idea that the entanglement spectrum of the ground state of a realistic Hamiltonian contains information not only about the universality class of the ground state but also about its excitations.

3.4 Particle entanglement spectrum

The concepts of entanglement entropy and entanglement spectrum are not specifically related to a partition in real space. Indeed, the OES is strictly speaking a partition in momentum space which in the specific case of the FQHE can be roughly related to a spatial cut. Partitioning a system in different ways can unveil different type of information, as it was shown in the case of quantum spin chains [28]. Among the possible partition, a simple one is based on removing particles from the system,

3 FRACTIONAL QUANTUM HALL EFFECT AND ENTANGLEMENT SPECTRA

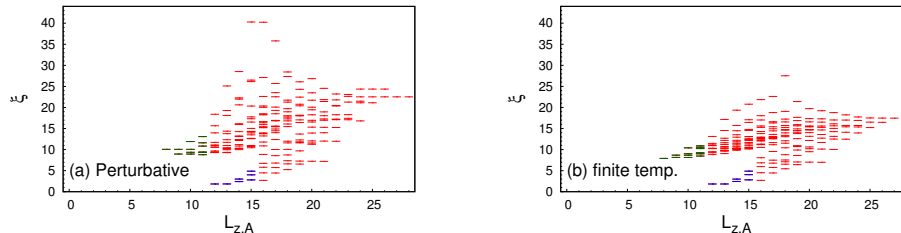


Figure 14: *Left panel:* OES from the linear combination of the $\nu = 1/3$ Laughlin state and the first neutral excitation having the same symmetry than the Laughlin state. For convenience, the linear combination is optimized to maximize the overlap with the Coulomb ground state. A fine tuning is not required to see that this technique reproduces the two lowest branches, indicating that the second branch (in green) is related to neutral excitations. *Right panel:* OES from the finite temperature calculation as defined in Eq. 21. We truncate the energy spectrum to only include the lowest energy neutral excitations (the magneto-roton mode). The temperature is set to $\beta = 7$ to mimic the OES of the Coulomb state. Once again, we clearly deduce that the second low entanglement energy branch is related to the lowest energy neutral excitations. For both figures, we use the same system sizes than Fig. 13.

realizing a particle partition. In the context of the entanglement entropy for FQHE, such a partition was introduced in Refs. [7] and [59]. The related entanglement spectrum, named the particle entanglement spectrum (PES), was introduced later in Ref. [60]. As opposed to the OES, the geometry (i.e. the number of orbitals) is preserved, the particles are divided into two groups A and B , holding respectively N_A and N_B particles. In first quantized notation and for a generic wave function $\Psi(x_1, \dots, x_N)$ for $N = N_A + N_B$ particles, the reduced density matrix is given by

$$\begin{aligned} \rho_A(x_1, \dots, x_{N_A}; x'_1, \dots, x'_{N_A}) \\ = \int \dots \int dx_{N_A+1} \dots dx_N \quad \Psi^*(x_1, \dots, x_{N_A}, x_{N_A+1}, \dots, x_N) \\ \times \Psi(x'_1, \dots, x'_{N_A}, x_{N_A+1}, \dots, x_N) \end{aligned} \quad (22)$$

As a first example, one can look at the completely filled lowest

Landau level, i.e. the $\nu = 1$ integer quantum Hall effect. The ground state on the sphere geometry for $N = N_\Phi + 1$ fermions is given by

$$|\Psi_{\nu=1}\rangle = \left| -\frac{N_\Phi}{2}, \dots, \frac{N_\Phi}{2} \right\rangle \quad (23)$$

This state is a product state in the orbital basis, leading to a trivial OES with a single non-zero eigenvalue. For the PES, the picture is different: The counting is given by the number of ways one can choose N_A particles among the N particles of the system. This case clearly stresses that different partitions probe different properties of the same system.

We now turn to the cases of interacting states, focusing on the Laughlin $\nu = 1/3$ state. Fig. 15a and b give the PES on the sphere and the disk geometry. As in the case of the OES, the counting is non-trivial (i.e. the number of non-zero eigenvalues is much lower than the naive dimension of the reduced density matrix) and does not depend on the geometry. What was empirically found in Ref. [60] is that the counting matches (per momentum sector) the number of quasihole states of the same state with N_A and N_Φ flux quanta (the particle partition does not affect N_Φ). This statement was checked for a large series of model wave functions. When these model wave functions are unique zero energy states of some local model Hamiltonian, one can prove that the counting is bounded by the number of quasihole states. Indeed, any eigenstate of ρ_A corresponding to a non-zero eigenvalue, has to be a quasihole state (meaning a zero energy state of the model Hamiltonian). Until now, there is no mathematical proof in the generic case that this bound has to be saturated. Note that the PES for $\nu = 1$ we have previously discussed above, can also be understood as the quasihole excitations of the integer quantum Hall state.

If we admit that the conjecture about the bound saturation is valid, then we completely understand the counting of the PES including any finite-size effect (as opposed to the OES). Both entanglement spectra, the OES and the PES, are actually related in the thermodynamical region [16]. In Fig. 15a, we give a schematic description of the quasihole states in each part of the PES. The leftmost angular momentum sector ($L_{z,A} = 0$) corresponds to the case where all quasiholes are located in the south hemisphere which is then completely depleted. We are left with a Laughlin droplet occupying the north hemisphere. Slightly

3 FRACTIONAL QUANTUM HALL EFFECT AND ENTANGLEMENT SPECTRA

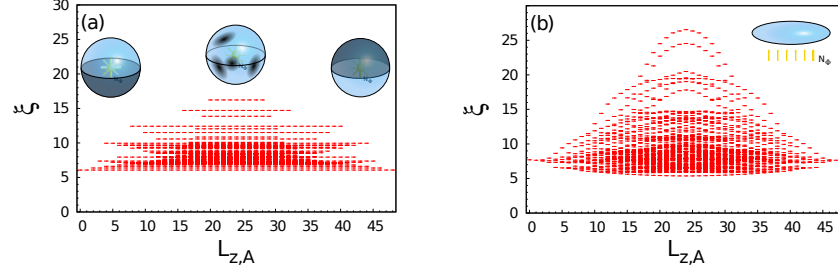


Figure 15: PES for the $\nu = 1/3$ Laughlin state with $N = 8$ fermions, $N_\Phi = 21$ and $N_A = 4$ on the sphere geometry (a) and on the disk geometry (b). In both cases, the counting per momentum is given by the number of quasihole states of the Laughlin state for N_A particles and $N_\Phi = 21$. The high degeneracy observed for the PES on the sphere is a consequence of the total angular momentum L_A^2 being a good quantum number when the PES is performed on a state with a total angular momentum equal to zero (such as the Laughlin ground state). For the sphere case, we schematically describe the types of quasihole states that correspond to the leftmost, center and rightmost levels.

moving away from $L_{z,A} = 0$ is equivalent to slight deformations of the droplet, i.e. the edge excitations. Indeed, the counting starting from $L_{z,A} = 0$ is $1, 1, 2, 3, \dots$ as expected from the Laughlin edge mode. Ref. [16] proved that the entanglement matrices (as defined in Sec. 2.1) associated with the thermodynamical region in both the PES and the OES must have the same rank. Using this bulk-edge (or PES-OES) correspondence, the proof of the Li-Haldane conjecture is reduced (at least for the class of model states that have been considered) to the proof of the bound saturation.

The PES can also be computed on the torus geometry. The FQH phases being topological phases, the degeneracy of their ground state changes with the genus of the surface they live on. For example on the torus, the Laughlin $\nu = 1/m$ state is m -fold degenerate and the Moore-Read state is 6-fold degenerate. Thus, multiple choices for the density matrix are available. For the PES, we use the incoherent density matrix

where one sums up all sectors:

$$\rho = \frac{1}{d} \sum_{i=0}^d |\Psi_i\rangle \langle \Psi_i| \quad (24)$$

where $\{|\Psi_i\rangle\}$ with $i = 1, \dots, d$ forms an orthogonal basis of the degenerate ground state manifold (d being the total degeneracy). As defined, this density matrix commutes with the magnetic translation operators and does not depend on a particular basis choice. The PES calculations are performed using the translation symmetry along one direction (here y), and the eigenvalues of ρ_A can be labeled by the corresponding $K_{y,A}$ momentum. Fig. 16a shows the PES for the Laughlin state on the torus. The properties are identical to those of the PES on the sphere: The counting matches the one of the quasihole states and the corresponding eigenstates of ρ_A span the subspace of the quasihole states. This is a clear difference with the OES on the torus where the counting is trivial as discussed in Sec. 3.2. For the ground state of the Coulomb interaction at $\nu = 1/3$, the PES is quite interesting: As observed in Fig. 16b, there is a clear entanglement gap separating a low entanglement energy structure having the same counting than the PES of the Laughlin and a higher entanglement energy part. From the different examples that have been studied, the PES behaves nicely on the torus geometry. This property will be used as a powerful tool to probe the physics of fractional Chern insulators in Sec. 4.

3.5 Real space entanglement spectrum

When we have described the OES in Sec. 3.2, we have argued that this type of partition was an approximation of a partition in real space, thanks to the specific properties of the orbital basis. The OES appears as a fuzzy cut and not a sharp cut. Several articles [20–22] have addressed the question of the real space entanglement spectrum (RSES) using a sharp real space partition. If one chooses a cut that preserves the rotation along z for the sphere or the disk, then $L_{z,A}$ is still a good quantum number. This makes the connection with the other ES easier. As in the case of the OES, N_A is also a good quantum number. A key property of the RSES is that a block of its entanglement matrix $M_{N_A}^{\text{RSES}}$ with a fixed N_A can be related to the entanglement matrix $M_{N_A}^{\text{PES}}$ of the PES for N_A particles. This relation is given by $M_{N_A}^{\text{RSES}} = S M_{N_A}^{\text{PES}} Q$

3 FRACTIONAL QUANTUM HALL EFFECT AND ENTANGLEMENT SPECTRA

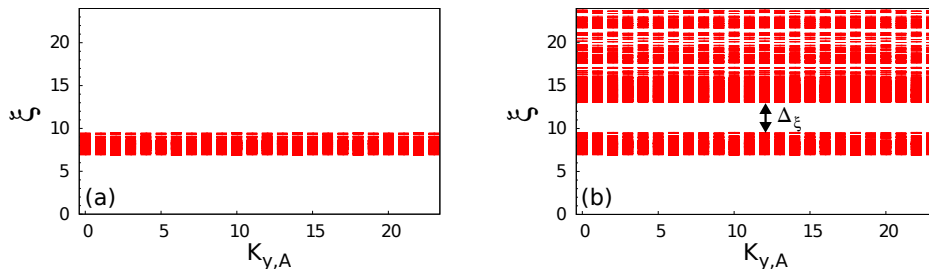


Figure 16: PES on the torus geometry for $N = 8$ fermions and $N_\Phi = 24$, keeping $N_A = 4$ particles. (a) The $\nu = 1/3$ Laughlin state. The counting per momentum sector is exactly given by the number of quasihole states with $N_A = 4$ fermions and $N_\Phi = 24$. (b) The Coulomb ground state. We observe a clear entanglement gap Δ_ξ between a low entanglement energy structure having the same counting than the PES of the Laughlin state and a higher entanglement energy part.

where S and Q are diagonal matrices with non-zero diagonal matrix elements. These elements are purely one-body geometrical factors coming from the space partition. As a consequence, the two matrices $M_{N_A}^{\text{PES}}$ and $M_{N_A}^{\text{RSES}}$ have the same rank and thus the two entanglement spectra have the same counting.

In Fig. 17a, we show the RSES of the $\nu = 1/3$ Laughlin state on the sphere when A is made of the north hemisphere, having a sharp cut at the equator. As expected the counting per momentum sector is identical to the one of the PES. The shape of the spectrum itself is reminiscent of the OES, being due to the geometrical cut. Beyond the counting, one could ask if the entanglement energies of RSES mimics the dispersion relation of the edge mode, in a better way than the OES. In both cases, the spread between the smallest and the largest entanglement energy in a given angular momentum sector seems to converge to zero. Fig. 17b gives the extrapolation of the average entanglement energy per angular momentum sector to the large number of particles limit. If in this limit the RSES was equivalent to the edge mode dispersion relation, we should expect these energies to be of the form $\frac{2\pi v}{\mathcal{L}}n$ where n is an integer, v is the edge mode velocity and \mathcal{L} is the cut perimeter. The finite size calculation has a roughly good agree-

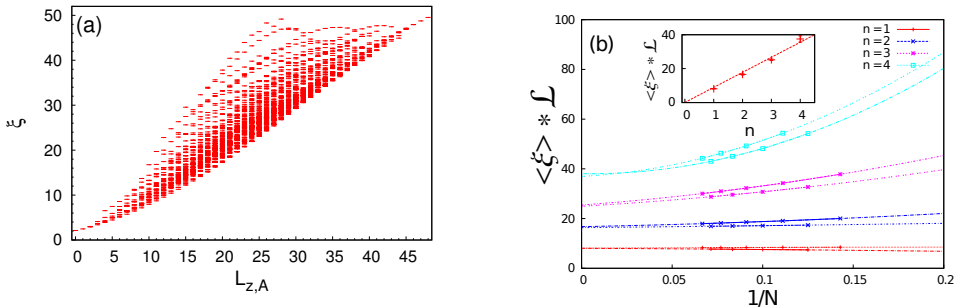


Figure 17: *Left panel:* RSES of the $\nu = 1/3$ Laughlin state on the sphere geometry for $N = 8$ fermions and $N_\Phi = 21$. We have used the (sharp) hemisphere cut and display the RSES in the sector $N_A = 4$. The counting is identical to the one of Fig. 15a. *Right panel:* The average entanglement energy $\langle \xi \rangle$ times the perimeter of the cut \mathcal{L} per momentum sector (here $n = L_z^A$) extrapolated at the thermodynamic limit as a function of $1/N$. The even-odd effect is just a consequence of N_A being the integer part of $N/2$. The velocity of the edge mode is $v = 1.41(5)$ (see inset). Such value would be compatible with a rescaling of the $\nu = 1$ edge mode velocity with a factor $1/\sqrt{3}$.

ment with this picture. Most of these properties have been recently confirmed in much larger system sizes using the MPS description of the Laughlin state [57]. These results underline once again that the ES of the system ground state contains the description of the edge excitations, reinforcing the bulk-edge correspondence.

4 Entanglement spectrum as a tool: Probing the Fractional Chern Insulators

As a practical application of the entanglement spectroscopy, we discuss the physics of Chern insulators in the strong interacting regime. We emphasize that the ES can conveniently replace the overlap calculations when those are not available. We show that the entanglement spectroscopy can discriminate between two phases where simple energetic analysis fails.

4.1 From Chern Insulators to Fractional Chern Insulators

Since their recent theoretical proposals [61–63] and their experimental discovery [64, 65], topological insulators have become a major topic in condensed matter physics—they are representative of a new class of materials which have been engineered to exhibit topological phases of matter. The first and simplest example of a topological insulator, the Chern insulator (CI), was introduced in a theoretical work by F.D.M. Haldane in 1988 [66]. It is defined by a non-zero Chern number C of the occupied bands. This (first) Chern number is a topological invariant, computed over the Brillouin zone, that characterizes a given band. A key feature is that a non-zero Chern number results [67] in a quantized Hall conductance $\sigma_{xy} = \frac{e^2}{h}C$, similar to the quantum Hall effect, but now without the requirement of a magnetic field.

A typical example of a Chern insulator is shown in Fig. 18. It is based on the Kagome lattice, a triangular lattice with three sites per unit cells, with a complex hopping term $t \exp(i\varphi)$ between neighboring sites. The Bloch Hamiltonian for this model is given by

$$\mathcal{H}(\mathbf{k}) = -t \begin{bmatrix} 0 & e^{i\varphi}(1 + e^{-ik_x}) & e^{-i\varphi}(1 + e^{-ik_y}) \\ & 0 & e^{i\varphi}(1 + e^{i(k_x - k_y)}) \\ \text{h.c.} & & 0 \end{bmatrix} \quad (25)$$

where $k_x = \mathbf{k} \cdot \mathbf{e}_1$ and $k_y = \mathbf{k} \cdot \mathbf{e}_2$, \mathbf{e}_1 and \mathbf{e}_2 are the lattice translation vectors as described in Fig. 18. The dispersion relation is displayed in Fig. 18, showing the three bands with two of them carrying a non-zero Chern number.

In the context of quantum Hall effect, strong interactions are known to give rise to the exotic physics of the fractional quantum Hall effect (FQHE). Current work suggests that, in an analog way to the FQHE, introducing strong interactions coupled with fractional filling of the topological insulator bands can give rise to novel and remarkable topological phases of matter. The first class of topological insulators that was studied in the strongly interaction regime was the Chern insulator. With the addition of strong interactions and fractionally filled bands these systems are known as fractional Chern insulators (FCI). At the beginning of 2011, several papers present evidence from numerical simulations [69–71] which demonstrated that FCIs could be implemented in principle for model systems.

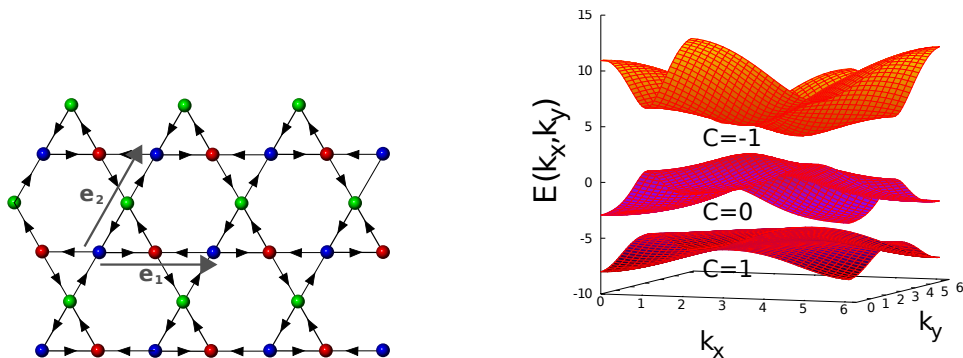


Figure 18: *Left panel:* The Kagome lattice model as discussed in Ref. [68] with three sites per unit cell. In the simplest case, this model has only a single complex nearest neighbor hopping term. *Right panel:* The band structure for the Kagome lattice model with a hopping term of $\exp(i\frac{\pi}{4})$. The topmost and the lowest band have a Chern number of $C = \pm 1$, while the middle band is trivial (i.e. a Chern number $C = 0$).

The simplest way to look at FCI is to work in the flat-band limit [71]: We focus on the interaction and the topological properties of the band structure, whereas the effect of band dispersion and band mixing are discarded. This allows to mimic the usual hypothesis of the FQHE calculations as described in Sec. 3.3. We start from the original Bloch Hamiltonian $\mathcal{H}(\mathbf{k}) = \sum_n E_n(\mathbf{k})P_n(\mathbf{k})$ where $E_n(\mathbf{k})$ and $P_n(\mathbf{k})$ are the dispersion and the projector onto the n -th band, respectively. Then we focus on the i -th band (like the lowest band for the case of the Kagome model) and consider the effective flat band Hamiltonian $\mathcal{H}_{\text{FB}}(\mathbf{k}) = P_i(\mathbf{k})$. From the energy perspective, this is the same situation than a single Landau level.

For the interacting case, we consider N spinless fermions on a lattice made of N_x unit cells in the \mathbf{e}_1 and N_y unit cells in the \mathbf{e}_2 with periodic boundary conditions. The filling factor is defined as $\nu = \frac{N}{N_x N_y}$. The simplest repulsive interaction that can be used for spinless fermions is just the nearest neighbor repulsive interaction

$$H_{\text{int}} = U \sum_{\langle i,j \rangle} : n_i n_j : \quad (26)$$

4 ENTANGLEMENT SPECTRUM AS A TOOL: PROBING THE FRACTIONAL CHERN INSULATORS

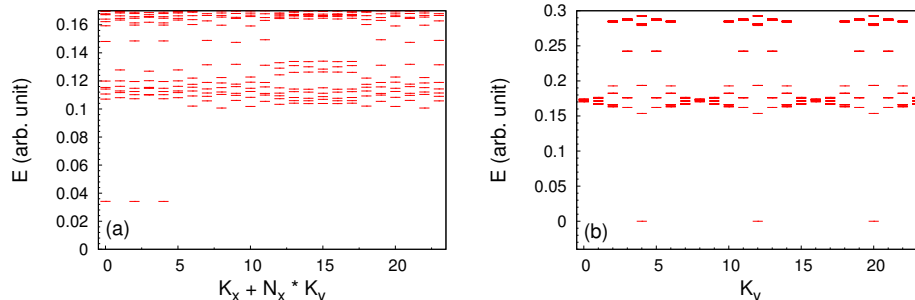


Figure 19: *Left panel:* Low energy spectrum for $N = 8$ fermions on a $N_x \times N_y = 6 \times 4$ unit cell Kagome lattice with periodic boundary conditions. K_x and K_y denote the total momentum in the x and y direction. We clearly observe an almost threefold degenerate ground state (the energy splitting between these three states is 3.1×10^{-5}). *Right panel:* Low energy spectrum for the FQHE with $N = 8$ fermions and $N_{\Phi} = 24$ on a torus. The Hamiltonian that we have used is the hollow core interaction for which the Laughlin state is the exact zero energy ground state.

where $\langle i, j \rangle$ denotes the sum over nearest neighboring sites. Projecting this interaction onto the lowest band and using the flat-band limit, the total effective Hamiltonian is just given by the projected interaction, similar to the FQHE case in Eq. 20. Exact diagonalizations can be performed to probe this system. A typical energy spectrum for the interacting Kagome lattice at filling factor $\nu = 1/3$ is shown in Fig. 19a. Similar to the FQHE on a torus (see Fig. 19b), we observe an (almost) threefold degenerate ground state clearly separated from the higher energy excitations. Note that the ground state is not exactly degenerate, as expected for the FQHE phase on a torus such as the Laughlin state. This is a consequence of the absence of an exact magnetic translation symmetry [72–74] as opposed to the FQHE.

Since Chern insulators are equivalent to quantum Hall systems without an external magnetic field, one could have imagined that FCIs should have given rise to topological phases analogous to those exhibited by the FQHE. Contrary to expectations, not all CI models [75] were found to exhibit such ‘fractional’ phases. For the time being, the emergence of FQH-like phases for a given model can only be probed

through numerical simulations of that given model. Moreover, many of the signatures obtained through the energy spectrum could also be obtained for charge density waves (CDW) in finite size calculations. As we will now discuss, the concept of entanglement spectrum has proved to be a power tool to probe these systems.

4.2 ES for FCI

FCI are lattice models and thus one could expect that performing a real space partition is rather trivial. The flat band procedure, which is done in momentum space, makes such a calculation rather non-trivial. Fortunately, the particle entanglement spectrum does not suffer from this issue and can be performed using this specific representation. Indeed, one can apply the same procedure than the FQHE on the torus that we have described in Sec. 3.4. We will use the same definition for the total density matrix than in Eq. 24, even if for FCI the degeneracy of the ground state is not exact. In Fig. 20, we present the PES for the almost threefold degenerate ground state of the Fig. 19a Kagome system. This PES, that can be plotted as a function of the momenta in both x and y directions, exhibits a clear and large entanglement gap. This PES is reminiscent of the one in Fig. 16b for the Coulomb ground state for the FQHE on a torus. The counting below this gap is exactly the one predicted for a Laughlin-like phase. One could wonder if an overlap calculation would have identified a Laughlin-like state. Writing the Laughlin state on FCI in a suitable way for numerical simulations was a difficult task [76, 77]. The results that have been obtained, confirmed what was already concluded from the PES.

Since these systems could also host CDW-like phases, one can wonder if such a phase would be detected by the PES. A simple way to force the system into a CDW phase consists to consider the one dimensional limit of a FCI [78], keeping only one unit cell in one direction (let say x here). For such a case, the signature from the energy spectra is actually quite similar to the one of a regular, two dimensional, FCI. For example, we still observe a threefold degenerate ground state at filling factor $\nu = 1/3$ (see Fig. 21a). Performing the PES gives a completely different perspective. As observed in Fig. 21b, there is still a large entanglement gap but the counting does not match the one expected for a Laughlin-like state. Indeed, it has been shown that this counting is the one of a CDW [78].

4 ENTANGLEMENT SPECTRUM AS A TOOL: PROBING THE FRACTIONAL CHERN INSULATORS

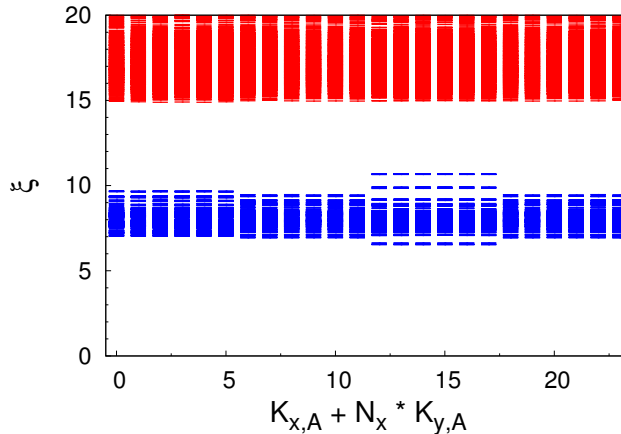


Figure 20: PES for using the three lowest energy states of the Kagome FCI model for $N_x \times N_y = 6 \times 4$, keeping $N_A = 4$ particles. $K_{x,A}$ and $K_{y,A}$ denote the total momentum in the x and y direction, and are good quantum numbers when performing the PES. There is a clear entanglement gap below which the number of levels (in blue) exactly matches the counting of Laughlin quasihole excitations on a system with 4 fermions on a system with $6 \times 4 = 24$ flux quanta. The counting per momentum sector below the entanglement gap matches the one predicted by the folding formula of Ref. [74].

As a last remark about ES for FCI, we point out that this technique was again quite successful to probe unusual phases. While FCIs share many common features with the FQHE, some striking differences make these systems host some new physics. The most remarkable example is that a single band can have a Chern number C higher than 1. Indeed, an usual single Landau level carries a Chern number equal to 1 and thus a completely filled Landau level has a Hall conductance equal to h/e^2 . This restriction does not apply to Chern insulators. The physics of non-interacting $C > 1$ is actually similar to C copies of a Landau level. These systems have been recently investigated numerically [79–82]. But the studies through ES [82, 83] have revealed that the picture of a simple multi-component FQH-like system breaks down when strong interactions are enabled.

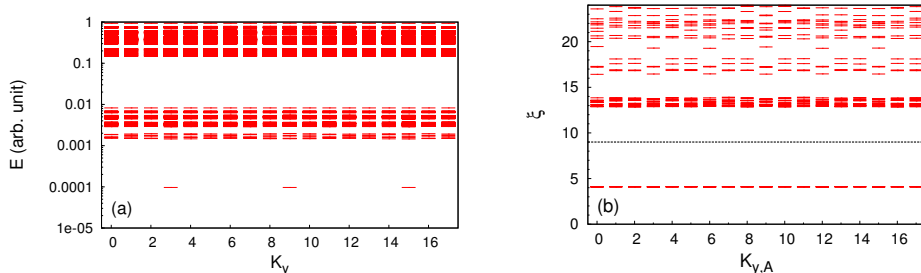


Figure 21: *Left panel:* The Kagome model in the one dimensional limit (i.e. $N_x = 1$) for $N = 6$ and $N_y = 18$. While we use a logarithmic scale for the energy, we still observe an almost threefold degenerate ground state. *Right panel:* PES for this almost threefold degenerate ground state, keeping $N_A = 3$ particles. There are 59 states per momentum sector below the entanglement gap (depicted by the black dashed line) as expected for a CDW (a Laughlin state would give 2530 states per momentum sector)

5 Conclusion

In this manuscript, we have reviewed the idea of entanglement spectroscopy. The most remarkable result of the ES is its ability to reveal how much information is encoded within many of the quantum ground states, even for finite size systems. Of course, relations between the ground state (the bulk of the system) and the low energy excitations (the edge modes) were already pointed out before the introduction of the ES. For model wave functions built from a CFT, the equivalence between the CFT of the bulk and the one associated with the edge was already conjectured in Ref. [54]. In a similar manner, using the reduced density matrix in strongly correlated systems is at the heart of the density matrix renormalization group [45]. The fundamental step made by Li and Haldane was to look at the data stored in the reduced density matrix in the right way, guided by the idea that the ES should mimic the energy spectrum of the edge modes.

The fractional quantum Hall effect was a nice sandbox where the concept of ES have been developed and tested. We have seen that several types of bipartition could allow to extract different types of information about the system excitations. While part of these results

REFERENCES

are still empirical, several steps have been made to give them a more robust analytical support. Maybe the most intriguing concept is still the one of the entanglement gap. For the FQH phases, there is a good understanding of the universal (or low entanglement energy) part. On the other hand, the “non-universal part” has also its own structure, related to neutral excitations. But there is still missing a quantitative understanding of the entanglement gap. How large should it be for a phase to be driven by the universal part? Future studies should address this issue.

In the early days of the ES, most of the results were derived from situations where many properties were already known (such as the case of model states). The recent works on fractional Chern insulators have proved that ES can be used as a tool to probe new systems. It helped to discriminate between different phases, especially when no expression for model states was available. Since computing the ES is generally a relatively straightforward numerical calculation, it should now be part of the toolbox used to analyze quantum systems. By picking the right quantum numbers, ES can be a powerful way to unveil the physics hidden in gigabytes of data.

References

- [1] D. C. Tsui, H. L. Stormer and A. C. Gossard, Two-dimensional magnetotransport in the extreme quantum limit, *Phys. Rev. Lett.*, **48**, 1559 (1982).
- [2] M. Levin and X.-G. Wen, Detecting topological order in a ground state wave function, *Phys. Rev. Lett.*, **96**, 110405 (2006).
- [3] A. Kitaev and J. Preskill, Topological entanglement entropy, *Phys. Rev. Lett.*, **96**, 110404 (2006).
- [4] P. Calabrese and J. Cardy, Entanglement entropy and quantum field theory, *J. Stat. Mech.*, P06002 (2004).
- [5] L. Amico, R. Fazio, A. Osterloh and V. Vedral, Entanglement in many-body systems, *Rev. Mod. Phys.*, **80**, 517 (2008).
- [6] M. Srednicki, Entropy and area, *Phys. Rev. Lett.*, **71**, 666 (1993).

-
- [7] M. Haque, O. Zozulya and K. Schoutens, Entanglement entropy in fermionic Laughlin states, *Phys. Rev. Lett.*, **98**, 060401 (2007).
- [8] A. M. Lauchli, E. J. Bergholtz and M. Haque, Entanglement scaling of fractional quantum Hall states through geometric deformations, *New. J. Phys.*, **12**, 075004 (2010).
- [9] H. Li and F. D. M. Haldane, Entanglement spectrum as a generalization of entanglement entropy: Identification of topological order in non-abelian fractional quantum Hall effect states, *Phys. Rev. Lett.*, **101**, 010504 (2008).
- [10] N. Regnault, B. A. Bernevig and F. D. M. Haldane, Topological entanglement and clustering of jain hierarchy states, *Phys. Rev. Lett.*, **103**, 016801 (2009).
- [11] O. S. Zozulya, M. Haque and N. Regnault, Entanglement signatures of quantum Hall phase transitions, *Phys. Rev. B*, **79**, 045409 (2009).
- [12] A. M. Läuchli, E. J. Bergholtz, J. Suorsa and M. Haque, Disentangling entanglement spectra of fractional quantum Hall states on torus geometries, *Phys. Rev. Lett.*, **104**, 156404 (2010).
- [13] R. Thomale, A. Sterdyniak, N. Regnault and B. A. Bernevig, Entanglement gap and a new principle of adiabatic continuity, *Phys. Rev. Lett.*, **104**, 180502 (2010).
- [14] R. Thomale, B. Estienne, N. Regnault and B. A. Bernevig, Decomposition of fractional quantum Hall model states: Product rule symmetries and approximations, *Phys. Rev. B*, **84**, 045127 (2011).
- [15] M. Hermanns, A. Chandran, N. Regnault and B. A. Bernevig, Haldane statistics in the finite-size entanglement spectra of $1/m$ fractional quantum Hall states, *Phys. Rev. B*, **84**, 121309 (2011).
- [16] A. Chandran, M. Hermanns, N. Regnault and B. A. Bernevig, Bulk-edge correspondence in entanglement spectra, *Phys. Rev. B*, **84**, 205136 (2011).
- [17] E. Ardonne and N. Regnault, Structure of spinful quantum Hall states: A squeezing perspective, *Phys. Rev. B*, **84**, 205134 (2011).

REFERENCES

- [18] A. Sterdyniak, B. A. Bernevig, N. Regnault and F. D. M. Haldane, The hierarchical structure in the orbital entanglement spectrum of fractional quantum Hall systems, *New Journal of Physics*, **13**, 105001 (2011).
- [19] Z. Liu, E. J. Bergholtz, H. Fan and A. M. Läuchli, Edge-mode combinations in the entanglement spectra of non-abelian fractional quantum Hall states on the torus, *Phys. Rev. B*, **85**, 045119 (2012).
- [20] A. Sterdyniak, A. Chandran, N. Regnault, B. A. Bernevig and P. Bonderson, Real-space entanglement spectrum of quantum Hall states, *Phys. Rev. B*, **85**, 125308 (2012).
- [21] J. Dubail, N. Read and E. H. Rezayi, Real-space entanglement spectrum of quantum Hall systems, *Phys. Rev. B*, **85**, 115321 (2012).
- [22] I. D. Rodriguez, S. H. Simon and J. K. Slingerland, Evaluation of ranks of real space and particle entanglement spectra for large systems, *Phys. Rev. Lett.*, **108**, 256806 (2012).
- [23] J. Schliemann, Entanglement spectrum and entanglement thermodynamics of quantum Hall bilayers at $\nu = 1$, *Phys. Rev. B*, **83**, 115322 (2011).
- [24] V. Alba, M. Haque and A. M. Läuchli, Boundary-locality and perturbative structure of entanglement spectra in gapped systems, *Phys. Rev. Lett.*, **108**, 227201 (2012).
- [25] P. Calabrese and A. Lefevre, Entanglement spectrum in one-dimensional systems, *Phys. Rev. A*, **78**, 032329 (2008).
- [26] F. Pollmann and J. E. Moore, Entanglement spectra of critical and near-critical systems in one dimension, *New Journal of Physics*, **12**, 025006 (2010).
- [27] F. Pollmann, A. M. Turner, E. Berg and M. Oshikawa, Entanglement spectrum of a topological phase in one dimension, *Phys. Rev. B*, **81**, 064439 (2010).
- [28] R. Thomale, D. P. Arovav and B. A. Bernevig, Nonlocal order in gapless systems: Entanglement spectrum in spin chains, *Phys. Rev. Lett.*, **105**, 116805 (2010).

-
- [29] A. M. Läuchli and J. Schliemann, Entanglement spectra of coupled $s = \frac{1}{2}$ spin chains in a ladder geometry, *Phys. Rev. B*, **85**, 054403 (2012).
- [30] H. Yao and X.-L. Qi, Entanglement entropy and entanglement spectrum of the kitaev model, *Phys. Rev. Lett.*, **105**, 080501 (2010).
- [31] J. I. Cirac, D. Poilblanc, N. Schuch and F. Verstraete, Entanglement spectrum and boundary theories with projected entangled-pair states, *Phys. Rev. B*, **83**, 245134 (2011).
- [32] I. Peschel and M.-C. Chung, On the relation between entanglement and subsystem hamiltonians, *EPL (Europhysics Letters)*, **96**, 50006 (2011).
- [33] C.-Y. Huang and F.-L. Lin, Topological order and degenerate singular value spectrum in two-dimensional dimerized quantum heisenberg model, *Phys. Rev. B*, **84**, 125110 (2011).
- [34] J. Lou, S. Tanaka, H. Katsura and N. Kawashima, Entanglement spectra of the two-dimensional affleck-kennedy-lieb-tasaki model: Correspondence between the valence-bond-solid state and conformal field theory, *Phys. Rev. B*, **84**, 245128 (2011).
- [35] J. Schliemann and A. M. Lauchli, Entanglement spectra of heisenberg ladders of higher spin, *Journal of Statistical Mechanics: Theory and Experiment*, **2012**, P11021 (2012).
- [36] L. Fidkowski, Entanglement spectrum of topological insulators and superconductors, *Phys. Rev. Lett.*, **104**, 130502 (2010).
- [37] E. Prodan, T. L. Hughes and B. A. Bernevig, Entanglement spectrum of a disordered topological chern insulator, *Phys. Rev. Lett.*, **105**, 115501 (2010).
- [38] A. M. Turner, Y. Zhang and A. Vishwanath, Entanglement and inversion symmetry in topological insulators, *Phys. Rev. B*, **82**, 241102 (2010).
- [39] Z. Liu, H.-L. Guo, V. Vedral and H. Fan, Entanglement spectrum: Identification of the transition from vortex-liquid to vortex-lattice

REFERENCES

- state in a weakly interacting rotating bose-einstein condensate, *Phys. Rev. A*, **83**, 013620 (2011).
- [40] J. Dubail and N. Read, Entanglement spectra of complex paired superfluids, *Phys. Rev. Lett.*, **107**, 157001 (2011).
- [41] R. B. Laughlin, Anomalous quantum Hall effect: an incompressible quantum fluid with fractionally charged excitations, *Phys. Rev. Lett.*, **50**, 1395 (1983).
- [42] I. Affleck, T. Kennedy, E. H. Lieb and H. Tasaki, Rigorous results on valence-bond ground states in antiferromagnets, *Phys. Rev. Lett.*, **59**, 799 (1987).
- [43] I. Affleck, T. Kennedy, E. H. Lieb and H. Tasaki, Valence bond ground states in isotropic quantum antiferromagnets, *Comm. Math. Phys.*, **115**, 477 (1988).
- [44] F. D. M. Haldane, Nonlinear field theory of large-spin heisenberg antiferromagnets: Semiclassically quantized solitons of the one-dimensional easy-axis néel state, *Phys. Rev. Lett.*, **50**, 1153 (1983).
- [45] S. R. White, Density matrix formulation for quantum renormalization groups, *Phys. Rev. Lett.*, **69**, 2863 (1992).
- [46] M. Fannes, B. Nachtergaele and R. Werner, Finitely correlated states on quantum spin chains, *Communications in mathematical physics*, **144**, 443 (1992).
- [47] D. Perez-Garcia, F. Verstraete, M. Wolf and J. Cirac, *Quantum Info. Comput.*, **7**, 401 (2007).
- [48] F. Verstraete, J. I. Cirac, J. I. Latorre, E. Rico and M. M. Wolf, *Phys. Rev. Lett.*, **94**, 140601 (2005).
- [49] J. I. Cirac and G. Sierra, Infinite matrix product states, conformal field theory, and the haldane-shastry model, *Phys. Rev. B*, **81**, 104431 (2010).
- [50] A. E. B. Nielsen, J. I. Cirac and G. Sierra, Quantum spin hamiltonians for the $su(2)$ k wzw model, *Journal of Statistical Mechanics: Theory and Experiment*, **2011**, P11014 (2011).

-
- [51] E. H. Rezayi and F. D. M. Haldane, Laughlin state on stretched and squeezed cylinders and edge excitations in the quantum Hall effect, *Phys. Rev. B*, **50**, 17199 (1994).
- [52] F. D. M. Haldane and E. H. Rezayi, Periodic Laughlin-Jastrow wave functions for the fractional quantized Hall effect, *Phys. Rev. B*, **31**, 2529 (1985).
- [53] F. D. M. Haldane, Fractional quantization of the Hall effect: A hierarchy of incompressible quantum fluid states, *Phys. Rev. Lett.*, **51**, 605 (1983).
- [54] G. Moore and N. Read, Nonabelions in the fractional quantum Hall effect, *Nuclear Physics B*, **360**, 362 (1991).
- [55] B. A. Bernevig and N. Regnault, The anatomy of abelian and non-abelian fractional quantum Hall states, *Phys. Rev. Lett.*, **103**, 206801 (2009).
- [56] Z. Papić, B. A. Bernevig and N. Regnault, Topological entanglement in abelian and non-abelian excitation eigenstates, *Phys. Rev. Lett.*, **106**, 056801 (2011).
- [57] M. P. Zaletel and R. S. K. Mong, Exact matrix product states for quantum Hall wave functions, *Phys. Rev. B*, **86**, 245305 (2012).
- [58] B. Estienne, Z. Papić, N. Regnault and B. A. Bernevig, Matrix product states for trial quantum Hall states, *Phys. Rev. B*, **87**, 161112 (2013).
- [59] O. S. Zozulya, M. Haque, K. Schoutens and E. H. Rezayi, Bipartite entanglement entropy in fractional quantum Hall states, *Phys. Rev. B*, **76**, 125310 (2007).
- [60] A. Sterdyniak, N. Regnault and B. A. Bernevig, Extracting excitations from model state entanglement, *Phys. Rev. Lett.*, **106**, 100405 (2011).
- [61] C. L. Kane and E. J. Mele, Quantum spin Hall effect in graphene, *Phys. Rev. Lett.*, **95**, 226801 (2005).
- [62] B. A. Bernevig, T. L. Hughes and S.-C. Zhang, Quantum spin Hall effect and topological phase transition in hgte quantum wells, *Science*, **314**, 1757 (2006).

REFERENCES

- [63] L. Fu and C. L. Kane, Topological insulators with inversion symmetry, *Phys. Rev. B*, **76**, 045302 (2007).
- [64] M. Koenig, S. Wiedmann, C. Brune, A. Roth, H. Buhmann, L. W. Molenkamp, X.-L. Qi and S.-C. Zhang, Quantum spin Hall insulator state in hgte quantum wells, *Science*, **318**, 766 (2007).
- [65] D. Hsieh, D. Qian, L. Wray, Y. Xia, Y. S. Hor, R. J. Cava and M. Z. Hasan, A topological dirac insulator in a quantum spin Hall phase, *Nature*, **452**, 970 (2008).
- [66] F. D. M. Haldane, Model for a quantum Hall effect without Landau levels: Condensed-matter realization of the “parity anomaly”, *Physical Review Letters*, **61**, 2015 (1988).
- [67] D. J. Thouless, M. Kohmoto, M. P. Nightingale and M. den Nijs, Quantized Hall conductance in a two-dimensional periodic potential, *Phys. Rev. Lett.*, **49**, 405 (1982).
- [68] E. Tang, J.-W. Mei and X.-G. Wen, High-temperature fractional quantum Hall states, *Phys. Rev. Lett.*, **106**, 236802 (2011).
- [69] D. N. Sheng, Z.-C. Gu, K. Sun and L. Sheng, Fractional quantum Hall effect in the absence of Landau levels, *Nat Commun*, **2**, 389 (2011).
- [70] T. Neupert, L. Santos, C. Chamon and C. Mudry, Fractional quantum Hall states at zero magnetic field, *Phys. Rev. Lett.*, **106**, 236804 (2011).
- [71] N. Regnault and B. A. Bernevig, Fractional chern insulator, *Phys. Rev. X*, **1**, 021014 (2011).
- [72] S. A. Parameswaran, R. Roy and S. L. Sondhi, Fractional Chern insulators and the W infinity algebra, *Phys. Rev. B*, **85**, 241308 (2012).
- [73] Goerbig, M.O., From fractional chern insulators to a fractional quantum spin Hall effect, *Eur. Phys. J. B*, **85**, 15 (2012).
- [74] B. A. Bernevig and N. Regnault, Emergent many-body translational symmetries of abelian and non-abelian fractionally filled topological insulators, *Phys. Rev. B*, **85**, 075128 (2012).

-
- [75] Y.-L. Wu, B. A. Bernevig and N. Regnault, Zoology of fractional chern insulators, *Phys. Rev. B*, **85**, 075116 (2012).
- [76] X.-L. Qi, Generic wave-function description of fractional quantum anomalous Hall states and fractional topological insulators, *Phys. Rev. Lett.*, **107**, 126803 (2011).
- [77] Y.-L. Wu, N. Regnault and B. A. Bernevig, Gauge-fixed Wannier wave functions for fractional topological insulators, *Phys. Rev. B*, **86**, 085129 (2012).
- [78] B. A. Bernevig and N. Regnault, Thin-Torus Limit of Fractional Topological Insulators, *ArXiv e-prints* (2012), 1204.5682.
- [79] Y.-F. Wang, H. Yao, C.-D. Gong and D. N. Sheng, Fractional quantum Hall effect in topological flat bands with chern number two, *Phys. Rev. B*, **86**, 201101 (2012).
- [80] S. Yang, Z.-C. Gu, K. Sun and S. Das Sarma, Topological flat band models with arbitrary chern numbers, *Phys. Rev. B*, **86**, 241112 (2012).
- [81] Z. Liu, E. J. Bergholtz, H. Fan and A. M. Läuchli, Fractional chern insulators in topological flat bands with higher chern number, *Phys. Rev. Lett.*, **109**, 186805 (2012).
- [82] A. Sterdyniak, C. Repellin, B. A. Bernevig and N. Regnault, Series of Abelian and Non-Abelian States in C_2 Fractional Chern Insulators, *ArXiv e-prints* (2012), 1207.6385.
- [83] Y.-L. Wu, N. Regnault and B. A. Bernevig, Bloch model wave functions and pseudopotentials for all fractional chern insulators, *Phys. Rev. Lett.*, **110**, 106802 (2013).